LBNL-45553

P-type doping of GaN

Raechelle Kimberly Wong

Center for Advanced Materials
Materials Sciences Division
Ernest Orlando Lawrence Berkeley National Laboratory
1 Cyclotron Road
Berkeley, California 94720

and

Department of Materials Science and Mineral Engineering
University of California
Berkeley, California 94720

M.S. Thesis

April 2000

This work was supported by the Director, Office of Science, Office of Basic Energy Sciences, Division of Materials Sciences, of the U.S. Department of Energy under Contract No. DE-AC03-76SF00098.

DISCLAIMER

P-type doping of GaN

by

Raechelle Kimberly Wong

B.S. (Carnegie Mellon University) 1997

A thesis submitted in partial satisfaction of the

requirements for the degree of

Master of Science
in

Engineering-Materials Science
and Mineral Engineering

in the

GRADUATE DIVISION

of the

University of California, Berkeley

Committee in charge:

Professor Eugene E. Haller, Chair
Professor Timothy D. Sands
Professor Roya Maboudian

Spring 2000

Table of Contents

Acknowledgements

Numerous people have contributed to the completion of my M.S. work, and from my experience, it is the people who set the tone of the work irrespective of the job itself. I have been fortunate that the students, scientists and staff in the Haller research group have been so generous with their time, knowledge and friendship.

It has been a rewarding experience working under the direction of Professor Eugene Haller. He has provided the support and resources for my research, as well as an enjoyable environment in which to work. I am grateful to Dr. Kin Man Yu for sharing his RBS expertise to help me understand the implantation damage in my samples. Much of my research also utilized PL, and I am particularly appreciative of the time Dr. Wei Shan and Steffen Kellerman spent teaching me the technique as well as having insightful discussions about our work. Bill Hansen and Jeff Beeman have been invaluable sources of lab expertise. Additionally, I would like to thank my fellow graduate students who shared with me all aspects of their lives and made our lab a great place to work.

I am most indebted to my parents for unconditionally supporting me and sacrificing for me. They have instilled in me the value and importance of education to achieve my dreams. Also, I am grateful to have my best friend Eric by my side, always willing to offer his time and help to support me in any endeavor I choose.

I would also like to thank Professor Tim Sands and Professor Roya Maboudian for reviewing this thesis. My research was made possible by Dr. Yong Chen at Hewlett-Packard who provided me with samples and by the University of California-Berkeley which assisted me financially with a fellowship. This work was supported by the

Director, Office of Science, Office of Basic Energy Science, Division of Materials Sciences of the U.S. Department of Energy under Contract No. DE-AC03-76SF00098.

1. Introduction

1.1 The rapid evolution of the group III-nitride semiconductor family

Research and development of the group III-nitride family of semiconductors have experienced explosive growth in the past decade. GaN, a wide direct bandgap semiconductor, and its alloys with AlN and InN, have realized, to a large degree their great promise in forming novel optoelectronic and high temperature devices. Development and fabrication of light emitting diodes (LED's) and laser diodes operating in the green to ultra-violet (UV) region, visible-(solar-)blind UV photodiodes and photoconductors, and high power, high temperature devices are currently being developed and some have already been realized.

GaN-based optical devices have practical uses in consumer electronics. In the green-blue region of the visible spectrum, these devices are already used in traffic lights and large full color flat panel displays. They provide cost savings through lower power consumption, long lifetimes and reduced maintenance. This may result in competitive alternatives to general-use overhead white lighting. Additionally, blue lasers have great promise for significant increases in storage densities in information storage media without requiring major technological changes to today's equipment.

Although some GaN-based products are already available commercially, there still exist serious limitations which have to be overcome for these devices to reach their full performance potential. For example blue laser lifetimes do not seem to improve, and Nichia Corporation, the leader in the field still does not offer any laser devices for sale. One of the limiting factors is the difficulty in obtaining low contact resistance ohmic contacts, particularly to p-GaN. This series resistance is detrimental to device performance, especially to the efficiency and lifetime of high current density devices such as lasers. This difficulty can be attributed to the lack of a truly shallow acceptor in GaN and the large work function of p-GaN.

1.2 Electrical behavior of metal/semiconductor junctions

When a metal and semiconductor come into contact, their Fermi levels have to coincide in the absence of an externally applied bias as shown in figures 1 and 2. Typically the work functions of the metal and the semiconductor are different which leads to band bending in the semiconductor. If a potential barrier to movement of majority carriers from the metal to semiconductor forms it is called a Schottky barrier. An ohmic contact is formed when there is no potential barrier or a negligible barrier to carrier flow in either direction. A potential barrier has a negligible influence on carrier flow if it is either very small, a few kT, or if it is very thin allowing efficient tunneling.

In p-type material, holes are the majority carrier. If a metal with work function (ϕ_m) smaller than that of the semiconductor work function (ϕ_s) is brought into contact with the semiconductor, the Fermi level of the metal is higher than the Fermi level of the semiconductor. Thus holes will flow from the semiconductor to the metal to lower hole energy states. On the semiconductor side of the junction, acceptor states become ionized (A^-) creating a region of negative space charge (Q_A^-). In the semiconductor, the conduction and valence bands bend downwards to prevent further movement of holes from the semiconductor to the metal until the Fermi levels align. At this point the flow of holes from the metal to the semiconductor and from the semiconductor to the metal are identical and typically very small. This situation is shown in figure 1.

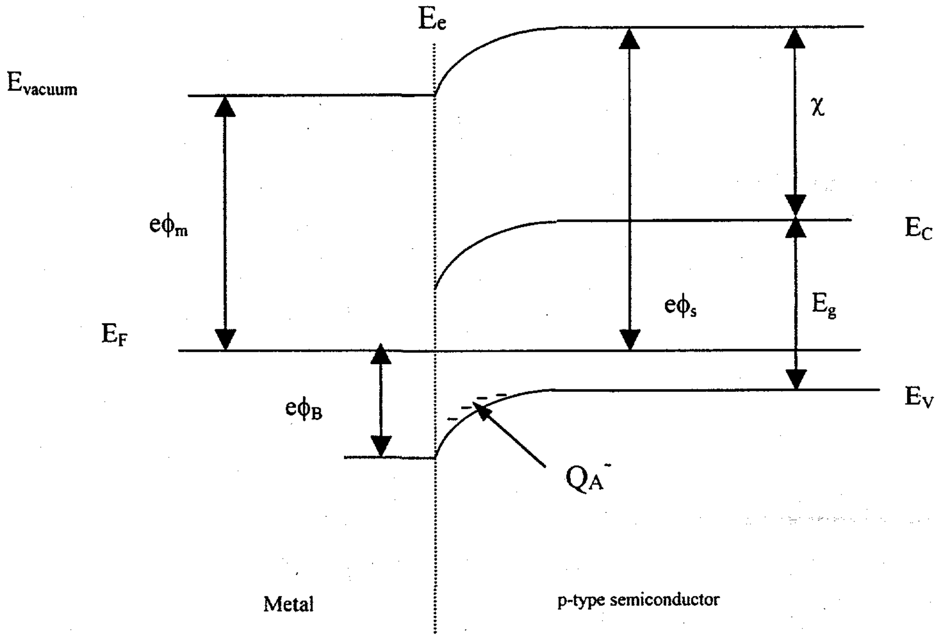

Figure 1. Formation of a Schottky barrier on a p-type semiconductor. ($\phi_m < \phi_s$)

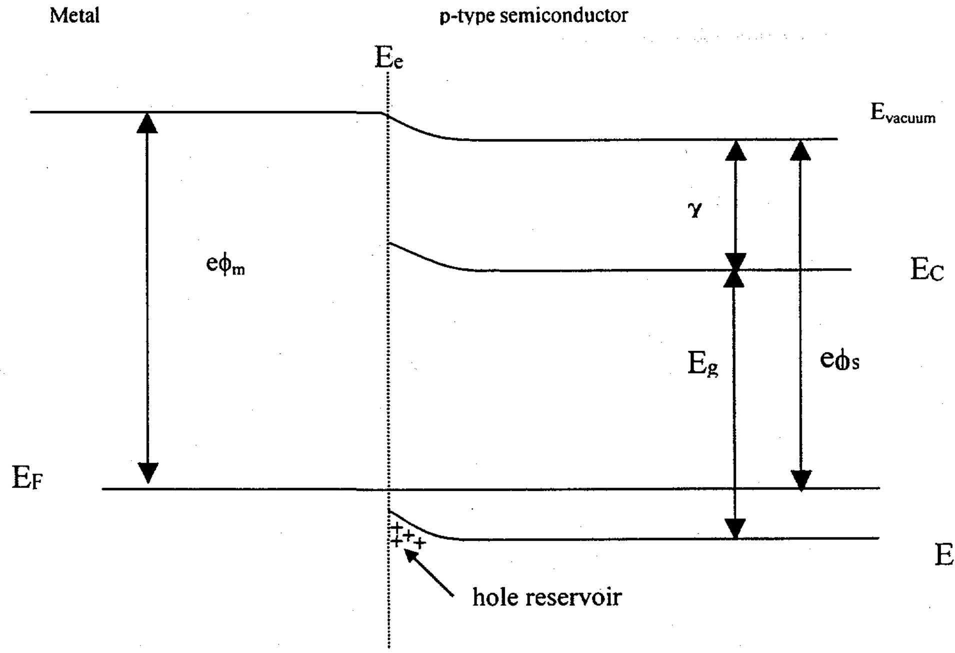

Figure 2. Formation of an Ohmic contact on a p-type semiconductor; no barrier to carrier flow. ($\phi_m > \phi_s$)

The barrier which forms is the Schottky barrier, ϕ_B, and, in its simplest form, is the difference between the metal work function, ϕ_m, and the semiconductor work function, ϕ_s; $\phi_B = \phi_m - \phi_s$.

On the other hand, if the metal work function is greater than the work function of the p-type semiconductor, ($\phi_m > \phi_s$), the Fermi level of the semiconductor is initially higher than the Fermi level of the metal. Thus holes will flow from the metal to the semiconductor to lower hole energy states, and the alignment of the Fermi levels will lead to band bending, but will not create an energy barrier to carrier movement. A hole reservoir forms on the semiconductor side as shown in figure 2. The effective barrier height is negligible and carriers are free to move over the barrier by thermionic emission in either direction as shown in figure 2. This situation allows large current injection upon application of an external bias with either polarity.

GaN has a bandgap energy, E_g, of 3.4 eV and an electron affinity, χ, of 4.1 eV. The electron affinity is defined as the energy from conduction band to the vacuum level, and the work function multiplied by e is the energy from the Fermi level to the vacuum level. In p-type material the Fermi level is located near the valence band, and in the case of GaN this would yield a semiconductor work function of ~7.5 eV. For a metal to form an ohmic contact to p-GaN, it must have a work function larger than ~7.5 eV. However metal work functions are typically well under 6 eV (see Appendix A), and ideally by this rule all metals will form Schottky contacts on p-type GaN.

The above discussion deals with the simplest model of barrier formation. However, factors such as surface states at the metal/semiconductor interface may play a role in determining barrier height. Surface states pin the Fermi level at a certain energy if the density of theses states is large enough. Then, the height of the barrier is no longer exclusively dependent on the difference between semiconductor and metal work functions. However, some studies have shown that the Fermi level at GaN surfaces may not be fully pinned at the surface, and that the Schottky barrier height is at least weakly dependent on the metal work function (Mori et al., 1996; Ishikawa et al., 1997). This suggests that a large work function metal should be used for the formation of ohmic or low barrier contacts on p-GaN.

It is apparent from reports in the literature that the simple work function model is not the sole factor influencing barrier heights at metal/p-GaN interfaces. A number of different contacts to p-GaN have been formed by a variety of metalization schemes: Pt/Au, Pd/Au and Ni/Au are just a few combinations that have been reported. In all of these cases the metal work function is smaller than 7.5 eV leading to some barrier. In the case of Ni-based contacts, it is believed that Ni reacts with the GaN surface forming a GaN:Ni alloy (D. Youn et al., 1998). Pd is believed to diffuse through the surface oxide contamination layer directly contacting the GaN surface (T. Kim et al., 1997). The more successful contact metals, however, appear to be those metals with the largest work functions.

1.3 P-type doping of GaN

Current technology utilizes the incorporation and activation of Mg impurities to form shallow acceptors in GaN. It was not until 1989 that p-type GaN by Mg doping was first realized by a post-growth low-energy electron-beam irradiation (LEEBI) treatment (Amano et al., 1989). Post growth annealing in a hydrogen free ambient was later found to have the same effects on Mg as the LEEBI treatment. Based on this finding, it was proposed that activation of the Mg acceptors was due to the dissociation and removal of H from electrically inactive Mg-H complexes. Far infrared (IR) spectroscopy was used to identify Mg-H and Mg-D local vibrational modes (LVMs) in as-grown and deuterated GaN thin films, verifying the passivation of Mg acceptors by H (Götz et al., 1996). The reduction in these LVM absorption peak heights was observed to be inversely proportional to the increased p-type conductivity in the films after an activation annealing step, a quantitative proof for the hydrogen passivation model.

Shallow dopants in a semiconductor can be described by modifying the equation for the binding energy of an electron bound to a proton (a hydrogen atom). Replacing the free electron mass and the dielectric constant with the effective mass of the electron or hole and the relative dielectric constant of the semiconductor leads to a very large reduction in binding energy. The binding energy of a shallow acceptor in a semiconductor using this so called "hydrogenic model" is given by

$$E = \frac{e^4 m_e}{2(4\pi\varepsilon_0 h)^2}\frac{m_h^*}{m_e}\frac{1}{\varepsilon_r^{\,2}} \qquad (1.1)$$

Applying equation 1.1 to GaN acceptors we find a value of E=190meV. This relatively large binding energy (large compared to kT at room temperature) is due to the large hole mass and the low dielectric constant of GaN. Because the energy level of the Mg acceptor is so deep, only about 1% of all Mg impurities occupying proper group III lattice sites is thermally ionized at room temperature. Hydrogen passivation or compensating native donor-like defects, such as N vacancies, can further reduce the concentration of active Mg acceptors. Therefore, high free hole concentrations in GaN are difficult to achieve, even for high acceptor concentrations. To attain the desired hole concentrations, it is necessary to be able to incorporate extremely large dopant concentrations in excess of 10^{20} cm^{-3}. A further difficulty is the low hole mobility, typical for compound semiconductors. The limited free hole concentration coupled with the low hole mobility results in resistive p-type material, a source of high power dissipation which leads to poor device performance. The 99% neutral Mg acceptors are to a limited degree responsible for the poor mobility because they contribute neutral impurity scattering. Fortunately, neutral impurities are not efficient scattering centers because there is no net-Coulomb field, and scattering caused by the neutral Mg acceptors is not expected to have a strong detrimental effect on the mobility.

1.4 Ohmic contacts

Low resistance ohmic contacts to a semiconductor are important for the operation of electronic devices, especially for all high current devices such as lasers. Current must be able to flow across the metal/semiconductor interface region without large voltage drops which cause heating and limit the device performance and lifetime.

Ohmic contacts on p-type material can be formed by two methods. The first method was discussed in the previous section on electrical behavior of metal/semiconductor junctions. It was shown that having a large work function metal with $\phi_m > \phi_s$ is necessary such that efficient carrier transport occurs by thermionic emission. The second approach to obtaining ohmic contacts is by reducing the width of depleted p-type material to a few tens of Angstroms such that carriers can quantum mechanically tunnel through the barrier by field emission. Tunneling occurs when the semiconductor surface region near the metal/semiconductor interface has a high ionized acceptor concentration. The high concentration of ionized acceptors causes the bands to bend more steeply, creating a thinner depletion region. The tunneling process is shown in figure 3b below for electrons across a Schottky barrier.

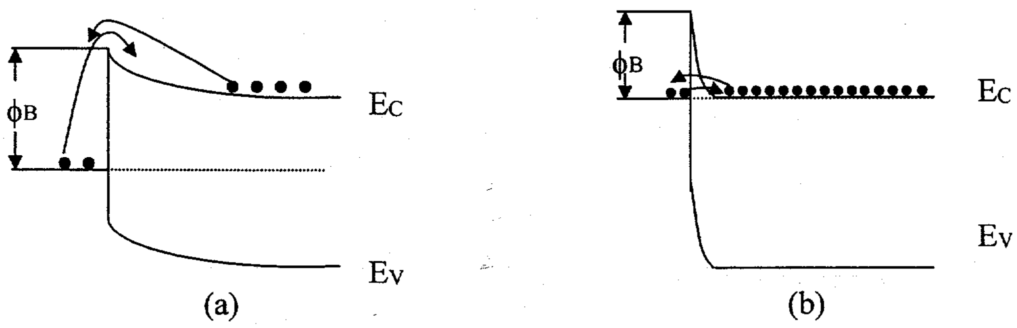

Figure 3. (a) lightly doped n-type semiconductor: electron transport by thermionic emission, no tunneling; (b) heavily doped n-type semiconductor: electron transport by field emission, tunneling dominates.

The specific contact resistance for contacts in which the tunneling process dominates is inversely proportional to the square root of the doping concentration as given in equation 1.2. By increasing the dopant concentration, the specific contact resistance decreases as shown by equation 1.2 (Murakami and Koide, 1998):

$$\rho_c = C_2 \exp\left[\frac{4\pi\sqrt{\varepsilon m^*}}{h}\left(\frac{\phi_B}{\sqrt{N_{dopant}}}\right)\right] \qquad (1.2)$$

In p-type material, N_{dopant} is the net ionized acceptor concentration. In the case of Mg-doped GaN, even though only ~1% of the net acceptor concentration is thermally ionized at room temperature in the bulk material, all uncompensated neutral Mg-acceptors will become ionized in the depletion region because the acceptor level lies below the Fermi level as shown in figure 4. Electrons at the Fermi level will fall to the lower energy acceptor level, thereby ionizing all the uncompensated acceptors.

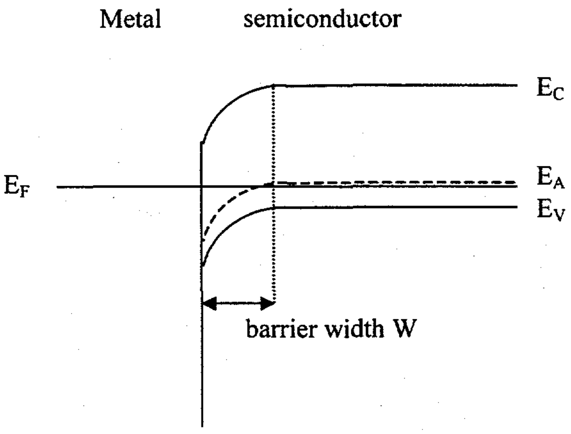

Figure 4. Metal-p-type semiconductor junction ($\phi_m<\phi_s$).

The barrier width can be calculated by equation 1.3.

$$W=\left[\frac{2\varepsilon V_0}{q}\left(\frac{1}{N_A^-}+\frac{1}{N_{metal\ ions}}\right)\right]^{1/2} \tag{1.3}$$

At a metal/semiconductor junction all of the depletion is assumed to be on the semiconductor side. As discussed earlier, all the uncompensated Mg acceptors will be ionized in the depletion region, therefore N_A^- is the net acceptor concentration. In our case this is typically $N_A^- \sim 3\text{x}10^{19}$ cm^{-3}. Using $\varepsilon=\varepsilon_r\varepsilon_0$ with ε_r=10.4 (Barker and Ilegems, 1973), $V_0=\phi_s-\phi_m$ = 1.85 V with Pt as the metal for the ideal case, and $N^+_{\text{metal ions}}$ = 6.64x10^{22} cm^{-3} as the density of electrons in Pt, the barrier width is calculated to be ~84Å. By increasing the acceptor concentration to 10^{20} cm^{-3}, the barrier width decreases to ~46 Å, a thickness through which efficient tunneling can occur.

1.5 Survey of alternatives to Mg for p-type doping of GaN

Due to the difficulties in obtaining large free hole concentrations and correspondingly low resistivities in p-GaN with Mg as the acceptor species, it is necessary to investigate elements other than Mg for their potential of forming shallow acceptors in GaN.

1.5.1 Investigation of Ca, Zn and Be

Experiments with Ca and Zn as alternative acceptors have been performed in the literature. By implantation of Ca alone and coimplantating with P, Ca was found to form an acceptor level with an ionization energy of ~169 meV (Zolper et al., 1996). Unfortunately, this value is very similar to the Mg acceptor ionization energy. Optical characterization by photoluminescence of Zn-doped GaN has shown spectral features indicating Zn acceptor levels (Pankove and Hutchby, 1976; Suski et al., 1998; Bergman et al., 1987). Bergman et al. (1987) used PL spectroscopy to assign Zn acceptors an ionization energy of 340 meV, which is much higher than that of Mg. Thus far, Zn doping has not led to hole conduction.

Recently, Be has been investigated as a potential p-type dopant. So far, only optical data have been reported for both MBE grown GaN:Be (Salvador et al., 1996; Sanchez et al., 1998; Dewsnip et al., 1998) and Be implanted GaN (Ronning et al., 1998). From assignments of Be-related levels to peaks in the photoluminescence spectra, energy levels from as little as ~90 meV to 250 meV above the valence band have been proposed.

First-principles calculations were performed on column I and column II elements as acceptors on the Ga-site in GaN (Neugebauer and Van de Walle, 1999). In this study of Li, Na, K, Be, Zn and Ca, only Be was found to be a viable alternative to Mg when considering solubility, possible interstitial formation and compensation as well as ionization energy. The calculated ionization energy for Be acceptors is slightly smaller than their result for Mg. However, the difference in the ionization energies lies within the error bars. A detrimental finding is that Be has the potential of being incorporated as an interstitial impurity because of its small size. As an interstitial impurity, Be is expected to be a double donor, and it will compensate Be_{Ga} acceptors.

First principles calculations were also made by Bernardini and Fiorenti (1997). They predict that Be forms an acceptor level in GaN with an ionization energy of only 60 meV, significantly smaller than that of Mg. Mireles and Ulloa (1998), using effective mass theory, also predict that Be forms an acceptor level in GaN shallower than the Mg level. However, their calculations predict a much smaller difference between the Mg and Be levels compared to the results by Bernadini and Fiorentini (1997), with Be forming a level 193-204 meV above the valence band as compared to their calculations for Mg at 204-215 meV above the valence band.

1.5.2 Additional aspects of Be in GaN

Based on all the theoretical work as well as on the experimental results, it is still rather uncertain whether or not Be forms a highly soluble shallow acceptor leading to highly conducting p-type GaN. The choice of Be as an acceptor will be discussed further here.

Like the other first row elements, Be has an incomplete first p-shell. This causes these elements to behave differently chemically and electrically in semiconductors as compared to their higher row element counterparts. For example, neither nitrogen in Ge nor oxygen in Si forms either single or double donors as would be expected from the behavior of group V and VI impurities in a group IV semiconductor. Instead of donating electrons to the semiconductor lattice, these impurities accept electrons to complete their first p-shell. Similarly in III-V semiconductors, O is not a shallow donor, and in GaN, O forms a deep level impurity which lies inside the conduction band rather than in the bandgap (Wetzel et al., 1997). The oxygen deep level emulates the generation of a free electron from a shallow donor when it self-ionizes from within the conduction band.

It has also been shown that the first row acceptor boron in Si is shallower than predicted by effective mass theory. The boron acceptor level lies merely 45 meV above the valence band, significantly shallower than the 70.5 meV predicted by effective mass theory (Baldereschi and Lipari, 1976). Boron slightly weakens the Coulomb potential binding the hole, and an extra electron is incorporated with two effects: the first is that the extra electron will complete the 4th bond with boron's four Si neighbors and the second is to further fill boron's first p-shell.

As for Be, it is possible that the weakening of the Coulomb potential also occurs, leading to a relaxed hole binding energy. Together with its high solubility expected from its behavior in other III-V compounds, this element may offer a promising alternative to Mg as a shallower acceptor.

1.5.3 Hydrogen co-doping

Several groups have discussed the use of hydrogen as an acceptor co-doping species to enhance acceptor activation of impurities. Van Vechten et al., (1992) discussed hydrogen co-doping of shallow dopant impurities in wide bandgap semiconductors to obtain high conductivity material. Their proposed approach was based on the premise that the free energy of a semiconductor is minimized when the Fermi level is at its intrinsic level. Making this assumption, he further postulated that under equilibrium conditions, the addition of shallow levels to the semiconductor, n-type or p-type, causes the crystal to create self-compensating native point defects to reduce its energy and maintain the minimum energy position of the Fermi level at the intrinsic level. (More recently Walukievicz (1998) showed that the formation energy for native defects has to be evaluated relative to the Fermi stabilization energy, E_{FS}, rather than the intrinsic Fermi level, and that E_{FS} in GaN is located in the upper part of the bandgap.) Thus there would be no net-gain of either n- or p-type conduction under these conditions. To remedy this situation, the introduction of hydrogen to neutralize the shallow dopants was proposed to avoid self-compensation (Van Vetchen et al., 1992; S. Nakamura et al., 1994; N. Johnson and D.P. Bour, 1996; J. Neugebauer and C.G. Van de Walle, 1994). Hydrogen H^+ species compensate A^- acceptors and H^- compensate D^+ donors forming neutral complexes in the semiconductor. Thus no effect on the Fermi level results from the passivated dopants, and as a consequence compensation by native defects is suppressed.

This theory of hydrogen passivation of shallow dopants supports observations in the activation of acceptors in p-GaN. During MOCVD growth, high concentrations of hydrogen are incorporated in GaN due to the hydrogen rich growth sources and the H_2 carrier gas. The as-grown Mg-doped GaN films are highly resistive. A post-growth electron irradiation treatment or thermal annealing in a hydrogen free environment is required to activate the Mg acceptors. This is a direct result of the removal of the passivating hydrogen species. Extrapolating from this fortuitous incorporation of hydrogen during MOCVD growth of Mg-doped GaN, intentional introduction of hydrogen into an acceptor doped semiconductor followed by removal of the hydrogen at energies or temperatures below the energy required to create native defects could result in large acceptor concentrations and high p-type conduction.

This method may be successful even in what would seem to be a non-equillibrium process such as ion implantation. Although the implantation process itself is a non-equilibrium technique, the damage created by implantation needs to be removed by high temperature anneals during which compensating defects can form. It is possible however to apply a non-equilibrium process such as rapid thermal annealing to reduce these unwanted and detrimental effects.

1.5.4 Si and O co-doping theories

Another approach to obtaining p-type doping with Be proposed by Yamamoto and Katayama-Yoshida (1997) is co-doping of Be (or Mg) with Si or O donors. Using ab initio electronic band structure calculations based on local-density-functional theory, they predicted that co-doping of acceptor dopants with donors "stabilizes" the charge distribution by reducing the Madelung energy. This "stabilization" of charge distribution is predicted to enhance acceptor incorporation and hole concentration in p-GaN. Indeed, p-type doping in cubic GaN was achieved through co-doping of Be with O (Brandt et al., 1996) with remarkably high free hole concentrations (10^{18} cm^{-3}) and hole mobility (150

cm^2/V s). However, no energy level of the Be acceptor was reported, and no further results have been published.

It is not obvious why the addition of compensating dopants should increase the net-dopant concentration. However, Yamamoto and Katayama-Yoshida's calculations indicate that the acceptor concentration can be increased by more than what is lost through compensation in the presence of compensating donors.

1.6 Ion implantation

Ion implantation is an essential method for doping semiconductors which is widely used in today's electronics industry. The ability to control the dopant concentration profile and dopant species as well as selectively implant submicron size areas by masking has rendered this technique indispensable in the fabrication of Si and compound semiconductor devices, especially integrated circuits.

The ion implantation process utilizes the ability to ionize almost any type of atom in either a gas or solid source, mass separate the ions of interest, accelerate and scan them homogeneously over a target. In general, the ions are accelerated to a potential on the order of 10's to 100's of kV such that they penetrate the target to 10's to 100's of nm.

The ions impinging into the sample are stopped by collisions or interactions in the semiconductor lattice that result in energy losses. There are two types of processes by which the ions come to rest in the host lattice, electronic and nuclear collisions. When the ion first enters the crystal with high energy, collisions between incident ions and electrons of the lattice atoms are the dominating loss process. However, because the mass of the electrons is so small, deviations from a straight ion trajectory are minimal.

These ion-electron collisions only cause small angle scattering. As the ions continue to lose energy through collisions with electrons, nuclear interactions caused by the interatomic potentials of the crystal atoms with the ions become important. The energy loss by nuclear interactions causes large scattering angles between the ions and the host atoms.

Some of the nuclear collisions create what is called radiation damage. This encompasses the displacement of host atoms by direct collisions with the incident ions as well as secondary collisions with recoiling atoms. To activate the dopant species both the removal of radiation damage and the movement of the dopant species onto proper substitutional lattice sites must occur. Generally this is accomplished by providing the energy necessary through thermal annealing.

1.6.1 Radiation damage in GaN

Numerous studies have been conducted to understand the radiation damage removal and activation of implanted impurities in GaN. Studies using channeling RBS and sheet resistance measurements of implanted Si forming donors are the most common and comprehensive found in the literature (Cao et al., 1998; Eiting et al., 1998; Tan et al., 1996, 1998; Zolper, 1997; Zolper et al., 1997, 1997, 1997, 1997, 1997, 1998). In the many studies made by Zolper et al. (1997, 1998) using progressively increasing annealing temperatures up to 1500°C, the activation of Si increased to levels as high at 88% and nearly full radiation damage recovery was observed after annealing at a temperature of 1500°C with a 15 kbar of N_2 overpressure. At 1 atm. ambient N_2 overpressure, full recovery of damage is not reached after annealing at 1400°C. Beyond 1400°C they found that their sputtered AlN film capping the GaN layers began to crack, reducing its effectiveness at preventing nitrogen loss. Other studies of Mg implanted GaN (N. Parikh et al., 1997) support the findings of Zolper et al.'s many studies with Si, Mg and Ca, showing that annealing at 1000°C was insufficient to fully recover the damage created during implantation.

Although complete recovery does not occur at temperatures under 1500°C, electrical activation of implanted dopants begins at lower temperatures. Zolper et al., found activation of Mg and Ca implanted species (co-implanted with P) at 1100°C and at 1050°C. They also found Si donor implants to be ~50% activated after 1100°C annealing which increased with further increasing the annealing temperature.

Table 1 below contains results compiled by Zolper et al. 1997, and it lists the activation temperature as a fraction of the absolute melting temperature for implants in specific semiconductors. For Si, GaSb, InP and GaAs, the annealing temperature required for optimal activation of implanted dopants is approximately 2/3 of the melting temperature.

The melting temperature of GaN is extremely high due to the high strength of the Ga-N interatomic bonds. It is theoretically predicted by use of Van Vechten's quantum dielectric theory of chemical bonding (Van Vechten, 1973) that the melting temperature of GaN is 2791 K (2518 °C) with 45 kbar of N_2 overpressure (S. Porowski et al, 1993). However, GaN decomposes by loss of N below 1000°C at 1 atmosphere pressure, far below the theoretical melting point. In order to maintain stoichiometric GaN at higher temperatures, extreme N_2 overpressures must be applied. Therefore, melting temperatures reported in the literature are the temperatures at which equilibrium of stoichiometric liquid and solid occurs with a given overpressure. Applying the rough 2/3 estimate to the T_m determined with 45 kbar of N_2 overpressure, maximum damage removal and implant activation is predicted to occur at a temperature on the order of ~1700°C.

semiconductor	Tm (°C)	Tact (°C)	Tact (°C)/Tm (°C)
Si	1415	950	0.67
GaSb	707	550	0.77
InP	1057	750	0.71
GaAs	1237	850	0.69
SiC	2797	1300-1600	0.46-0.57
GaN	2518*	~1700	0.67

Table 1. Implant activation temperature in relation to melting temperature in select materials. (from Zolper et al., 1997) *Theorectically predicted value for a N_2 overpressure of 45 kbar.

1.6.2 Co-implantation

In addition to thermal annealing used to activate implanted dopant species, it was shown previously in GaAs that the activation of an implanted low-mass element such as C can be significantly enhanced. This was achieved by co-implanting a heavier element with the same depth profile that also maintains the III-V stoichiometry (Moll et al., 1993). In this work, C was implanted to form an acceptor occupying an As site. The heavier co-implanted species induced greater damage in the crystal which resulted in improved substitution of C atoms on the As site. Additionally, co-implanting with a high mass group III element like Ga further improved the activation of the C_{As}. By creating an excess of atoms on the group III sublattice, the C preferentially moved to the group V sites improving the C on As site substitution as well as the stoichiometry of the crystal. The increase in free hole concentration with increasing co-implant mass as well as with a species which maintained crystal stoichiometry is shown in figures 5 and 6.

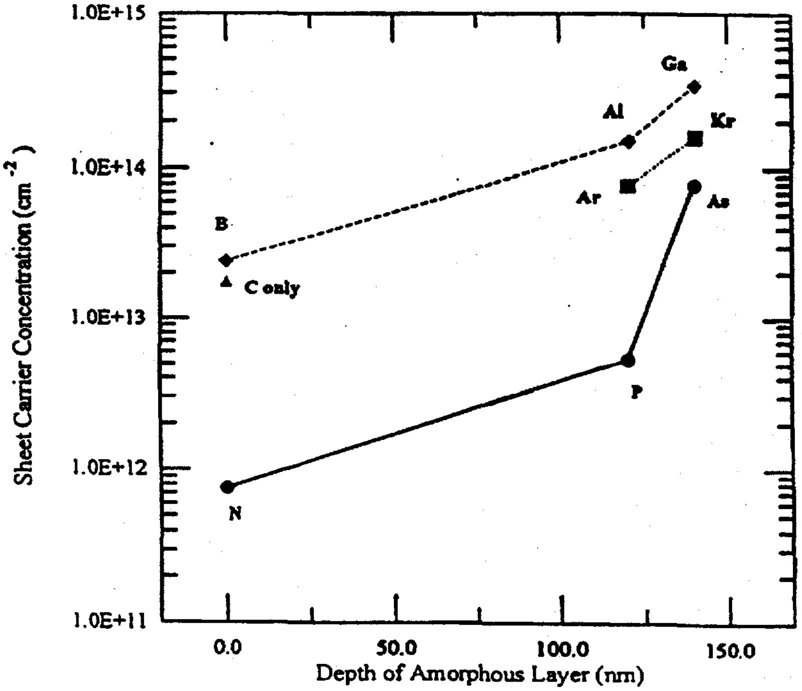

Figure 5. Free hole concentration as measured by Hall effect as a function of the depth of the amorphous layer as measured by RBS. (Moll et al., 1993)

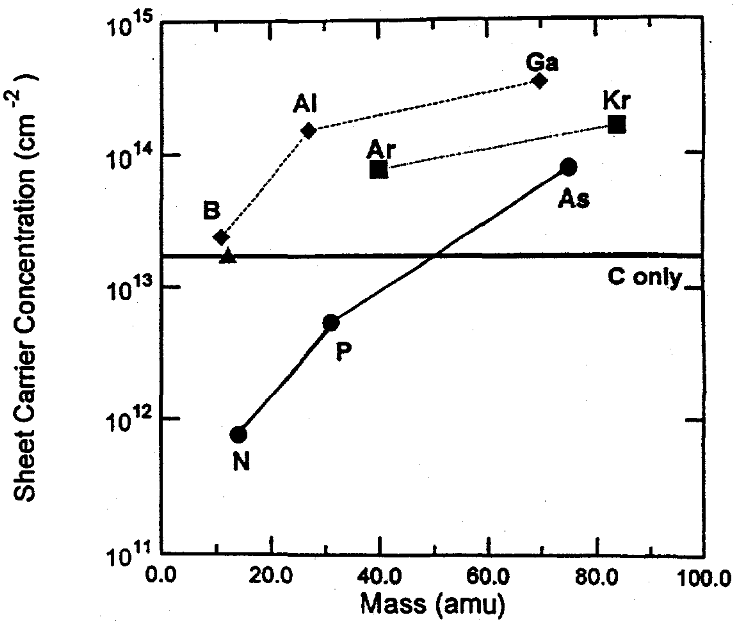

Figure 6. Sheet carrier concentration as a function of the atomic mass of the co-implant species. Samples were annealed at 950°C for 10 s. (Moll et al., 1993)

In the work with Be which is described in detail in this thesis, this scheme of co-implanting a heavier mass element which would maintain stoichiometry is employed. Although the work with GaAs cannot be directly transferred to GaN, it is worthwhile to study this co-implantation technique for the implantation of light mass elements like Be in GaN.

1.6.3 AlN encapsulating layers

The annealing of GaN at high temperatures causes decomposition of the GaN surface through loss of nitrogen. Nitrogen vacancies created by N loss at the surface is expected to create a highly n-type surface layer. In p-type material, n-conduction at the surface due to N vacancies can over compensate the acceptor levels. This would be counterproductive to creating a heavily p-type near surface region. By annealing in vacuum, significant loss of N was already observed below 1000°C by mass spectrometry (Groh et al., 1974). By providing overpressures of N_2, nitrogen loss from the surface can be suppressed or at least reduced. This can be accomplished by flowing N_2 gas during thermal annealing or by providing an appropriate amount of N_2 backpressure for samples sealed and annealed in ampoules. However, ambient nitrogen overpressure only prevents surface decomposition up to ~1200°C; above this temperature not only does the surface degrade, but with increasing temperatures the entire film decomposes (Pearton et al., 1999). Sample annealing in N_2 at an overpressure of 1.6 GPa increased the maximum temperature below which GaN decomposition was suppressed to 1500°C (T. Suski et al., 1998). Unfortunately utilization of such high pressure is not a conventionally available application.

A sputtered encapsulating or capping layer of AlN has been found to prevent nitrogen loss from the GaN surface to temperatures exceeding 1300°C (Pearton et al., 1999). AlN protects the GaN surface because it has a higher dissociation temperature. The choice of AlN as a cap is also convenient because AlN can be removed by selectively etching in hot KOH solutions (J.R. Mileham et al., 1995). Thus, to preserve the integrity of the GaN surface and layer during the high temperatures necessary to remove implant damage, an AlN capping layer must be used.

2. Experimental Procedures

2.1 Sample origin and processing

2.1.1 Sample origin

The GaN thin film samples used in these studies were obtained from Dr. Yong Chen at the Hewlett Packard laboratories in Palo Alto, CA. The GaN epilayers were grown on c-plane oriented sapphire by metal organic chemical vapor deposition (MOCVD). The GaN films were Mg-doped with a post-activation room temperature free hole concentration of $\sim 3.1\text{x}10^{17}$ cm^{-3}, sheet resistivity of $\sim 1.8\text{x}10^{4}$ Ωcm, mobility of ~ 6.0 cm^2/Vs and thickness of $\sim 1.8\mu\text{m}$.

2.1.2 Ion implantation

All samples with the exception of a single p-GaN sample used as a control were implanted with Be + As, As + Ga or simply As. Ion implantation of all implant species was performed commercially. Samples were mounted on a Si wafer with Kapton tape. The wafers were tilted 7° from normal to avoid channeling during implantation. Co-implantation was performed such that the implant profile of the co-implant species overlapped the first implant species profile as shown in figure 7.

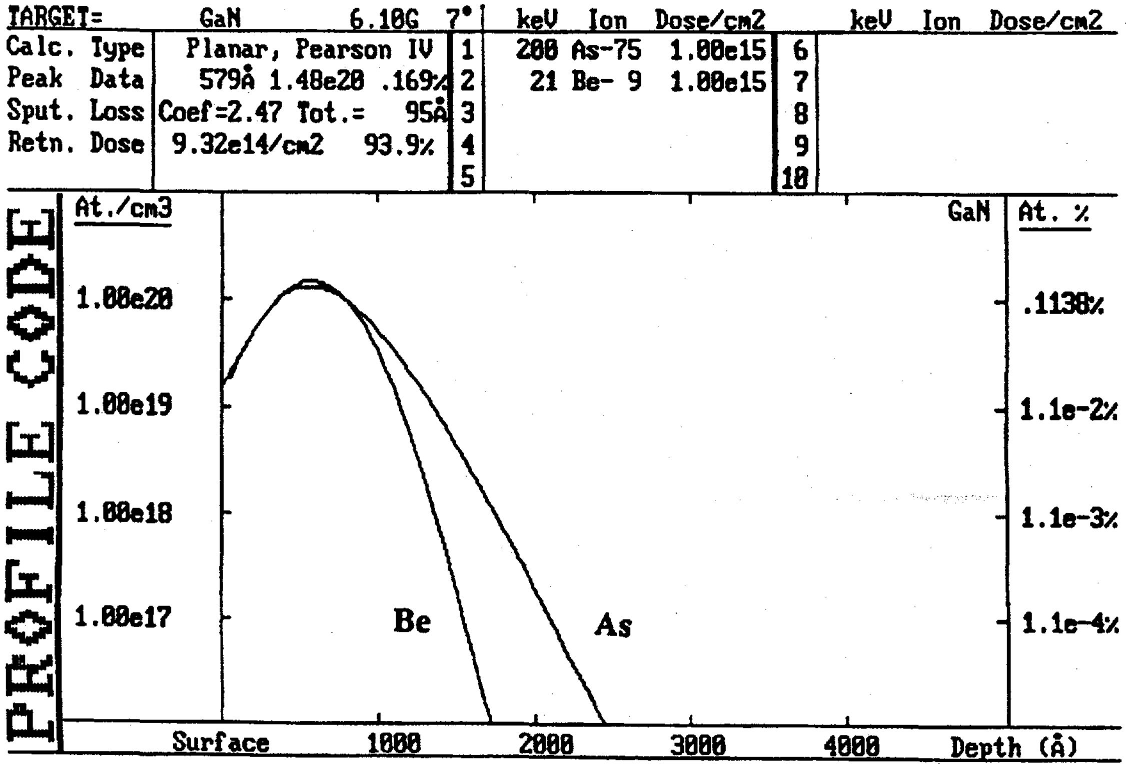

```
TARGET=        GaN          6.10G  7° | keV  Ion    Dose/cm2      keV  Ion   Dose/cm2
Calc. Type | Planar, Pearson IV | 1 | 200 As-75  1.00e15 | 6
Peak  Data |   579Å 1.48e20 .169% | 2 |  21 Be- 9  1.00e15 | 7
Sput. Loss |Coef=2.47 Tot.=   95Å | 3 |                    | 8
Retn. Dose | 9.32e14/cm2   93.9% | 4 |                    | 9
           |                    | 5 |                    |10
```

Figure 7. Beryllium (21 keV) co-implanted with Arsenic (200 keV) into GaN.

2.1.3 Hydrogen Passivation

Some samples were subjected to a hydrogen passivation step either following implantation or after initial annealing. A radio frequency (RF) plasma system was used to generate a hydrogen plasma in which the samples were hydrogenated. The samples were placed in a graphite crucible which was heated by 0.5 MHz RF power to 600°C for 1 hour. A 13.57 MHz RF generator was used to excite the plasma. H_2 flows through a bubbler filled with water to reduce recombination of hydrogen with the walls of the quartz tube (Wood, 1922). During cooling of the samples, the hydrogen plasma was sustained. A schematic of the hydrogenation system used is shown in figure 8.

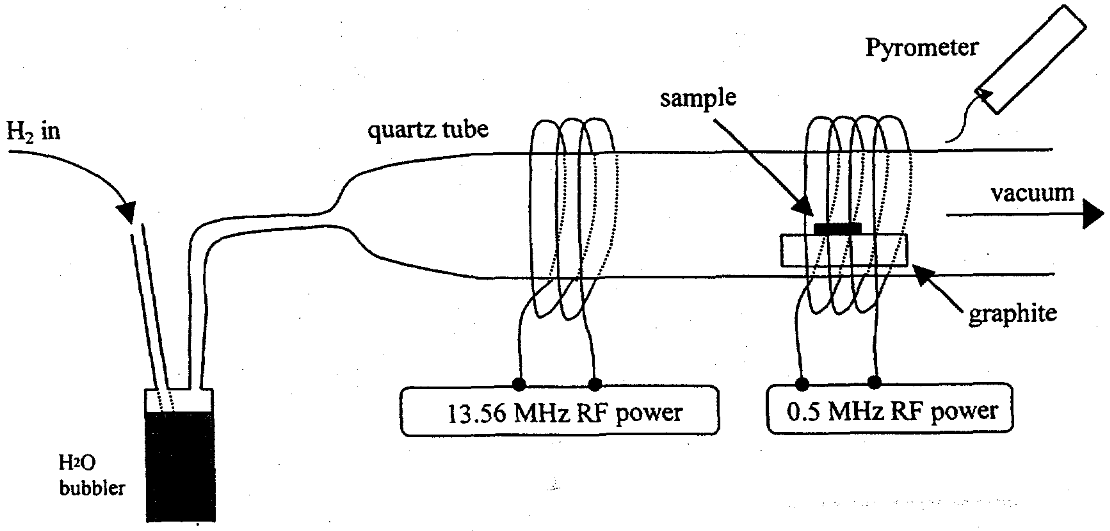

Figure 8. Schematic of RF plasma hydrogenation system.

2.1.4 Surface Preparation

Immediately prior to contact metal deposition, AlN cap deposition or hydrogen passivation, all samples were prepared to minimize sample surface contamination. Samples were first degreased in a series of boiling solvents: xylenes, acetone and methanol, for 3 minutes each. This was followed by a 5 minute wet etch to reduce the oxygen at the surface. A dilute, buffered oxide etch (BOE) solution composed of 1 part BOE and 10 parts deionized (DI) water was used for this purpose (K. Duxstad, 1997). BOE is 6 parts NH_4F and 1 part DI water. Samples were then rinsed in DI water and blown dry with N_2.

2.1.5 AlN cap and metal contact deposition

To prevent decomposition of the GaN film and loss of N from the surface during high temperature annealing, an AlN film was sputter deposited as a capping layer prior to most annealing runs (Zolper et al., 1997). AlN was sputter deposited on the sample surfaces in a Perkin-Elmer model 2400 sputtering system. A gas mixture of 80% Ar and 20% N was used. The Al target was pre-sputtered for 3 hours prior to cap deposition to ensure the oxide on the surface of the Al target was removed and to reduce background oxygen and water contamination. Pre-sputtering occurred at a forward power of 300 W at 10 mTorr gas pressure. The oxide on the Al target was assumed to be removed when the target bias, initially at 800W, increased to above 1000W. Load and tune settings were readjusted to minimize the reflected power after the oxide was sputtered off the Al target. The AlN cap was sputter deposited for 6 minutes 20 seconds, approximately 100 nm, at a forward power of 250 W in a gas pressure of 7 mTorr.

From Rutherford backscattering spectrometry (RBS), the maximum oxygen incorporation in the AlN films sputtered at these conditions was found to be less than 10%.

To perform Hall effect resistivity measurements contacts were deposited in a Veeco electron beam evaporator. Pt/Au contacts were deposited followed by annealing at 750°C for 10 minutes in a N_2 atmosphere.

2.1.6 Thermal Annealing

All implanted samples were thermally annealed to remove implant damage and move implanted species onto substitutional lattice sites. Samples were sealed in quartz ampoules, backfilled with N_2 such that the pressure in the ampoule at the desired annealing temperature would be 1 atmosphere. Prior to use, ampoules were cleaned in a 5% HF solution.

Samples sealed in ampoules were annealed in a Blue M Rad-O-Glow globar ceramic furnace constructed such that a quartz tube could be vertically placed into the furnace. This allowed the sample to be rapidly immersed in the furnace preheated to the annealing temperature. A schematic of the furnace set up is shown in figure 9. The furnace was heated to the specific annealing temperature before ampoules containing the samples were dipped into the furnace. Samples were annealed at temperatures ranging from 900°C to 1500°C. Following annealing, the ampoules were removed from the furnace, quenched with a quick spray of water and then placed in ethylene glycol. Misting of the ampoules with water was done to reduce the temperature of the ampoule to below the flash point of ethylene glycol.

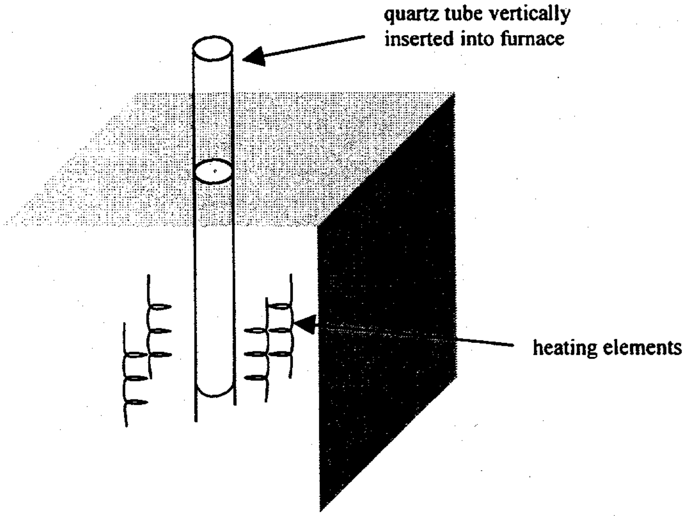

Figure 9. Schematic of vertical box furnace with quartz tubing inserted vertically into furnace.

2.2 Sample Characterization

To understand changes in the material due to processing steps, the GaN samples were characterized prior to implantation and after major processing steps. Appendix C gives a detailed description of each of the characterization techniques used. Since the main goal of this work was to introduce electrically active acceptors, Hall Effect and resistivity measurements were made to determine the electrical properties of the material, and photoluminescence (PL) was performed to study optical transitions and properties. Channeling Rutherford backscattering spectrometry (c-RBS) was performed mainly to analyze damage created due to ion implantation and its removal during thermal annealing. RBS was also used to characterize the oxygen content and thickness of the sputtered AlN capping layers. Secondary ion mass spectrometry (SIMS) was also performed commercially to verify implantation and hydrogen diffusion profiles as well as to determine the impact of annealing on species diffusion either from the cap, from the substrate or within the layer.

2.2.1 Hall effect and resistivity

Room temperature Hall effect measurements were performed to determine the concentration of free carriers in the GaN layers. The epilayer must be either electrically isolated from the substrate or the substrate must be insulating to perfom accurate measurements. The latter condition was satisfied in our studies because the GaN layer was grown on a sapphire substrate. To form contacts, Pt/Au films were electron beam evaporated at the four corners of each square sample. Contact deposition was followed by annealing at 750°C for 10 minutes in flowing N_2. Contact to the Hall effect apparatus was made by copper wires which were attached to the Pt/Au contacts with cold pressed Indium.

A high impedance system was used to obtain accurate electrical measurement for samples with resistances as high as several time 10^{10} Ω. These values are significantly lower than the system limit of 10^{14} Ω.

A magnetic field of 0.3 Tesla was used for all Hall measurements to determine the free carrier concentration. Resistivity was also measured in the same system, and from this measurement and the free carrier concentration, the free carrier mobility was calculated. A more detailed description of the Hall effect system and method used in these studies can be found in Appendix 6.3.1.

2.2.2 Photoluminesence (PL)

Photoluminesence studies were conducted at ~12K using a He-Cd laser with a laser line wavelength of 325.8 nm as an excitation source and a spot size of approximately 150 μm in diameter. Samples were mounted using vacuum grease in a cryostat and cooled to ~12K with a closed cycle He refrigerator consisting of a He compressor and a cooling head. Radiative emission of photons from the sample was focused through 2 lenses through a 1mm wide slit into a 1 meter double grating spectrometer and into a Hamamatsu 928 multi-alkali photomultiplier tube. A photomultiplier with lock-in amplification system was used to improve the signal to noise ratio. A more detailed description of the PL technique can be found in Appendix 6.3.2.

2.2.3 Channeling Rutherford backscattering spectrometry (c-RBS)

C-RBS was utilized to analyze implantation damage recovery with annealing. C-RBS measurements were made with a 1.92 MeV He^+ beam. The ions were accelerated by a Van de Graaff accelerator and then focused and collimated. The beam with a spot size of ~1 mm in diameter was then directed onto the sample. In channeling experiments, the sample was oriented precisely along the <0001> axis. The 15 nA incoming beam was positioned along the sample normal with a scattering angle of 80° to the Si surface barrier detector. About 10 μC of charge were collected for each spectra. A random spectrum was taken of the unimplanted virgin p-GaN sample as a reference spectrum. Backscattered ions were analyzed by energy with a solid state Si surface barrier detector which had a solid angle of detection of approximately 2 msr. The pulses were sorted by energy in a multichannel analyzer. Secondary electrons were suppressed by a shield biased at –900V which encircled the sample. The details of the c-RBS method can be found in Appendix 6.3.3.

2.2.4 Secondary ion mass spectrometry (SIMS)

SIMS analysis was performed to determine a number of concentration profiles. For example, we checked if oxygen diffusion from the AlN cap into the GaN layer had taken place. Ion implant and dopant species concentration distribution as a function of annealing were analyzed by SIMS as well. SIMS analysis was performed commercially by the Materials Analysis Group in Sunnyvale, CA, a division of Accurel System International Corporation.

A CAMECA IMS-3f double-focusing mass spectrometer instrument was used to perform SIMS analysis. Cesium ions formed the primary beam with an energy of ~9 keV either with positive or negative polarity to enhance negative and positive ejected secondary ions respectively. Secondary ions or ionized molecules ejected from the samples were accelerated away from the surface with a voltage of 4500 V into the mass spectrometer for detection. A more detailed description of SIMS can be found in Appendix 6.3.4.

3. Experimental results

3.1 Radiation damage removal

Radiation damage created by ion implantation and its removal by annealing was studied by channeling RBS. By comparing the number of backscattered ions from channeling of implanted samples to channeling of the as-grown film and to the random RBS spectrum, the degree of crystallinity can be determined. GaN films were implanted with 10^{15} cm^{-2} As (As), 10^{15} cm^{-2} As + 10^{14} cm^{-2} Be (AsBe14), 10^{15} cm^{-2} As + 10^{15} cm^{-2} Be (AsBe15) and 10^{15} cm^{-2} As + 10^{15} cm^{-2} Ga (AsGa). All implants were performed such that the peak implant concentration was ~800Å deep. Further implant details are given in appendix B. During thermal annealing, all samples with the exception of the ones annealed at 900°C, were capped with a sputtered AlN film approximately 100nm thick which contained no more than ~10% oxygen.

Figure 3.1 shows channeling RBS spectra of the as-implanted and as-grown films, as well as a random spectrum for comparison. The channeling results show that with implantation, damage accumulates at depths extending from ~200Å to ~1100Å as well as at the surface. The accumulated damage further from the surface will be referred to as the "main" damage peak. The main damage peak originates from displaced Ga atoms, and integration of this peak yields the number of displaced Ga atoms. It is evident that no implant schedule created a completely amorphous layer, as no portion of the channeled spectra coincided with the random spectrum.

It is expected that more and heavier implanted ions will create a greater amount of radiation damage in the film. The c-RBS spectra in figure 3.1 reflect this trend, with the film implanted with 10^{15} cm^{-2} As ions showing the least amount of damage both in the main damage peak as well as at the surface. Increasing the number of implanted ions from just $10^{15}\ \mathrm{cm}^{-2}$ As to also include $10^{14}\ \mathrm{cm}^{-2}$ Be ions, increased the disorder in the film. Implantation of $10^{15}\ \mathrm{cm}^{-2}$ As and $10^{15}\ \mathrm{cm}^{-2}$ Ga created even more disorder in the film, showing that the heavier implant impurities cause greater in-plane damage, evidenced by the increase in damage peak height, as well as larger damage depth, shown by the larger damage peak width. Although c-RBS was not performed on the sample implanted with $10^{15}\ \mathrm{cm}^{-2}$ As and $10^{15}\ \mathrm{cm}^{-2}$ Be, it is expected that the damage concentration in this sample is slightly more than the damage in the film implanted with $10^{15}\ \mathrm{cm}^{-2}$ As and $10^{14}\ \mathrm{cm}^{-2}$ Be, but less than the film implanted with As and Ga.

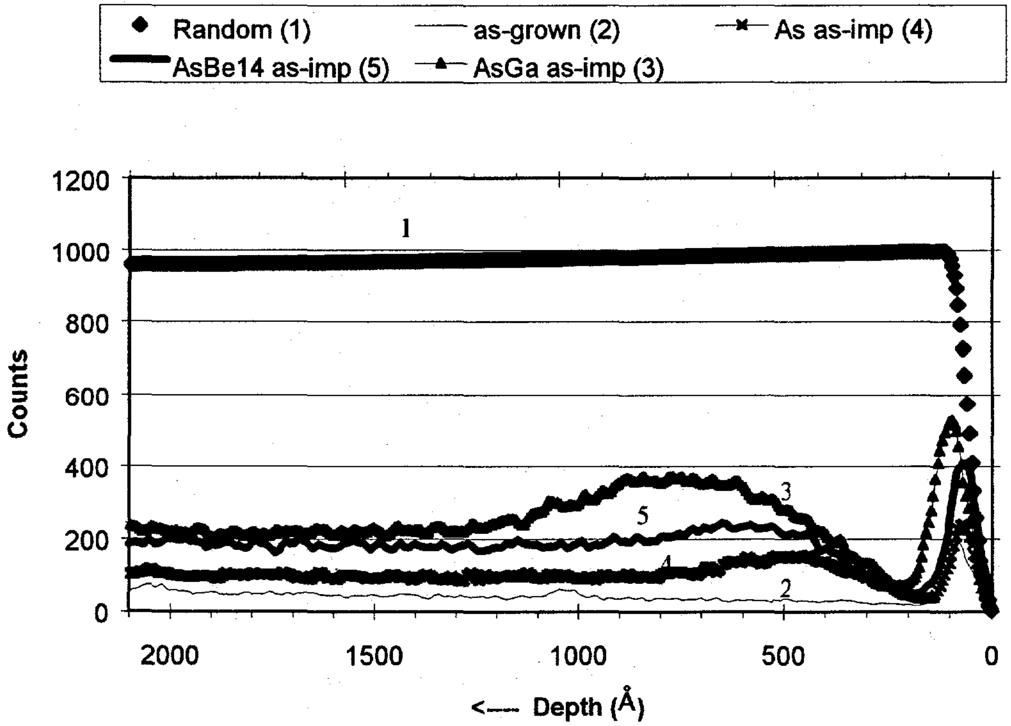

Figure 3.1. 1.92 MeV He$^+$ <0001> aligned RBS spectra of GaN layers implanted with As ($10^{15}\ \mathrm{cm}^{-2}$), with As ($10^{15}\ \mathrm{cm}^{-2}$) + Ga ($10^{15}\ \mathrm{cm}^{-2}$) and with As ($10^{15}\ \mathrm{cm}^{-2}$) + Be ($10^{14}\ \mathrm{cm}^{-2}$).

Figure 3.2a shows damage recovery of films implanted with only As after thermal annealing. Annealing at 1400°C for 30s shows slight recovery of radiation damage. In comparison to the as-implanted spectra there is a small reduction in both the main and surface damage peaks. Annealing at 1500°C for 30s significantly reduces the main damage peak height and depth, but even after such high temperature annealing, the damage is still not fully recovered. The surface peak, however, slightly increases compared to the sample annealed at 1400°C for 30s. Figure 3.2b shows the surface peaks in larger detail. The increase in damage at the surface may be an indicator that the AlN cap was no longer fully effective at 1500°C and decomposition of the GaN surface occurred

Damage recovery of AsBe14 implanted samples with thermal annealing is shown in figure 3.3. After annealing at 900°C for 10 minutes, there is a significant reduction in both the main and surface damage peaks. There is a reduction in the amount of displaced Ga atoms as well as a reduction in the damage depth from ~900Å to ~700Å. Annealing the implanted sample at 1400°C for 30s slightly reduces the damage further in the main damage and surface damage areas over annealing at 900°C for 10 minutes. It appears that after annealing at 1400°C for 30s, there is nearly full recovery of radiation damage.

The RBS spectra of the AsBe15 implanted and annealed samples are shown in figure 3.4. C-RBS was not performed on the as-implanted AsBe15 sample, and the as-implanted AsBe14 spectrum was plotted as a reference, which slightly underestimates the actual damage. Unlike the AsBe14 sample annealed at 1400°C for 30s, the AsBe15 sample did not show nearly full recovery after annealing under the same conditions. Comparing this sample to the as-implanted AsBe14 sample, there is some damage recovery in the main damage area. After annealing at 1500°C for 30s there is considerable reduction in the main and surface damage peaks. The surface damage peak did not rise above the surface peak for the sample annealed at 1400°C for 30s as it did in the As implanted samples. Again, recovery is incomplete even after annealing at 1500°C for 30s.

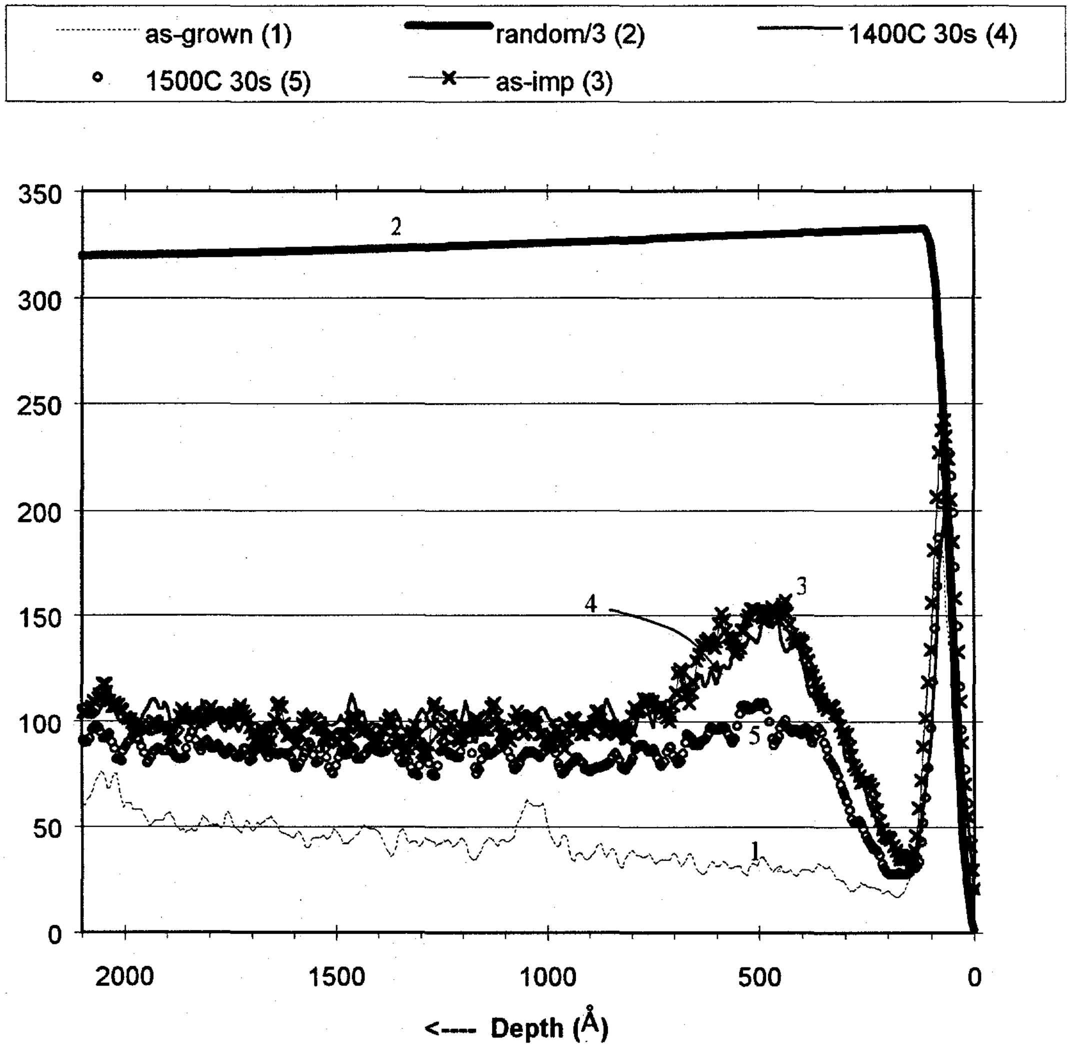

Figure 3.2a. 1.92 MeV He^+ <0001> aligned RBS spectra of GaN layers implanted with As (10^{15} cm^{-2}) with different annealing treatments.

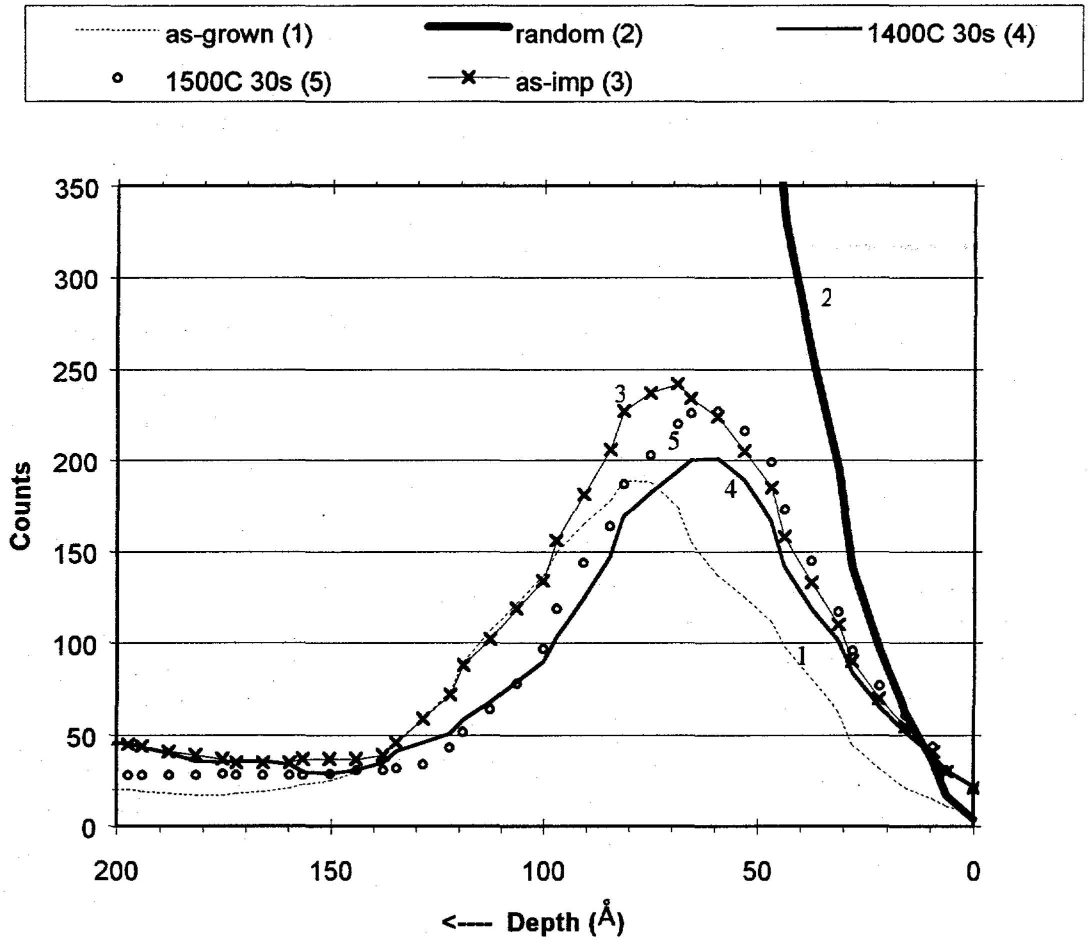

Figure 3.2b. Detail of surface damage peak from 1.92 MeV He^+ <0001> aligned RBS spectra of GaN layers implanted with As (10^{15} cm^{-2}) with different annealing treatments.

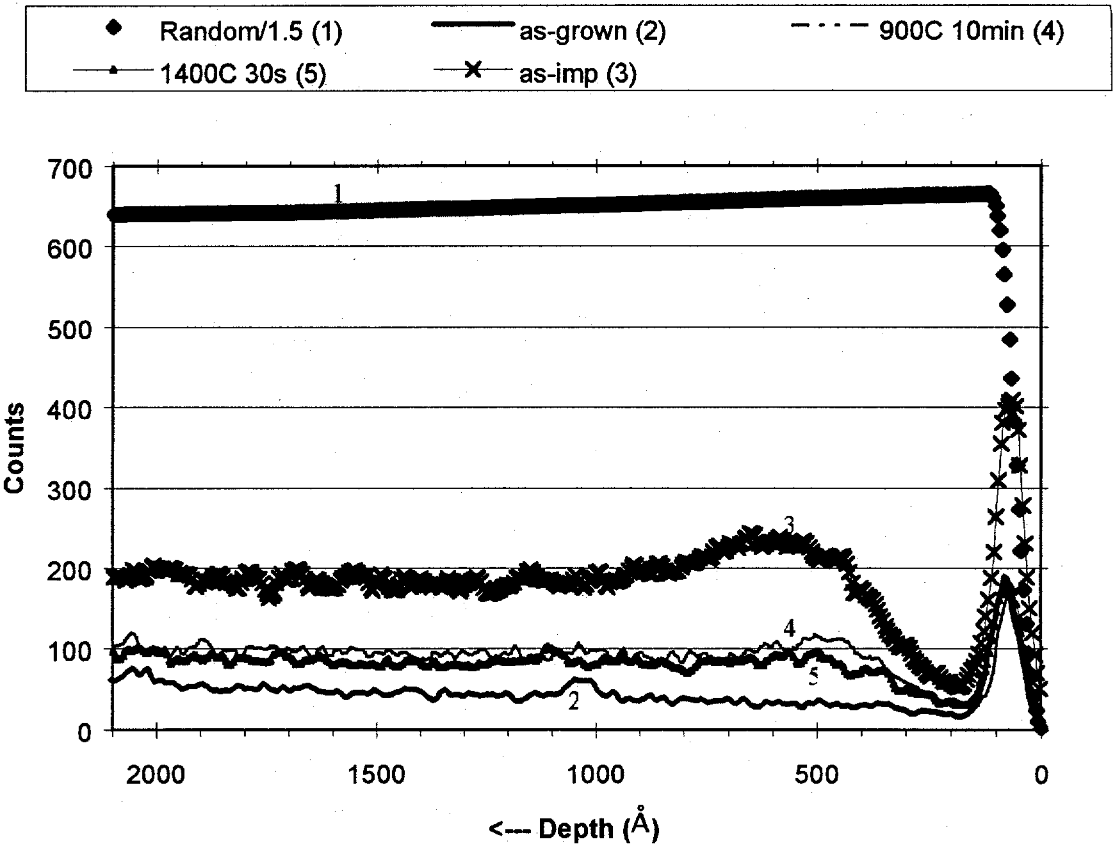

Figure 3.3. 1.92 MeV He^+ <0001> aligned RBS spectra of GaN layers implanted with As (10^{15} cm^{-2}) and Be (10^{14} cm^{-2}) with different annealing treatments.

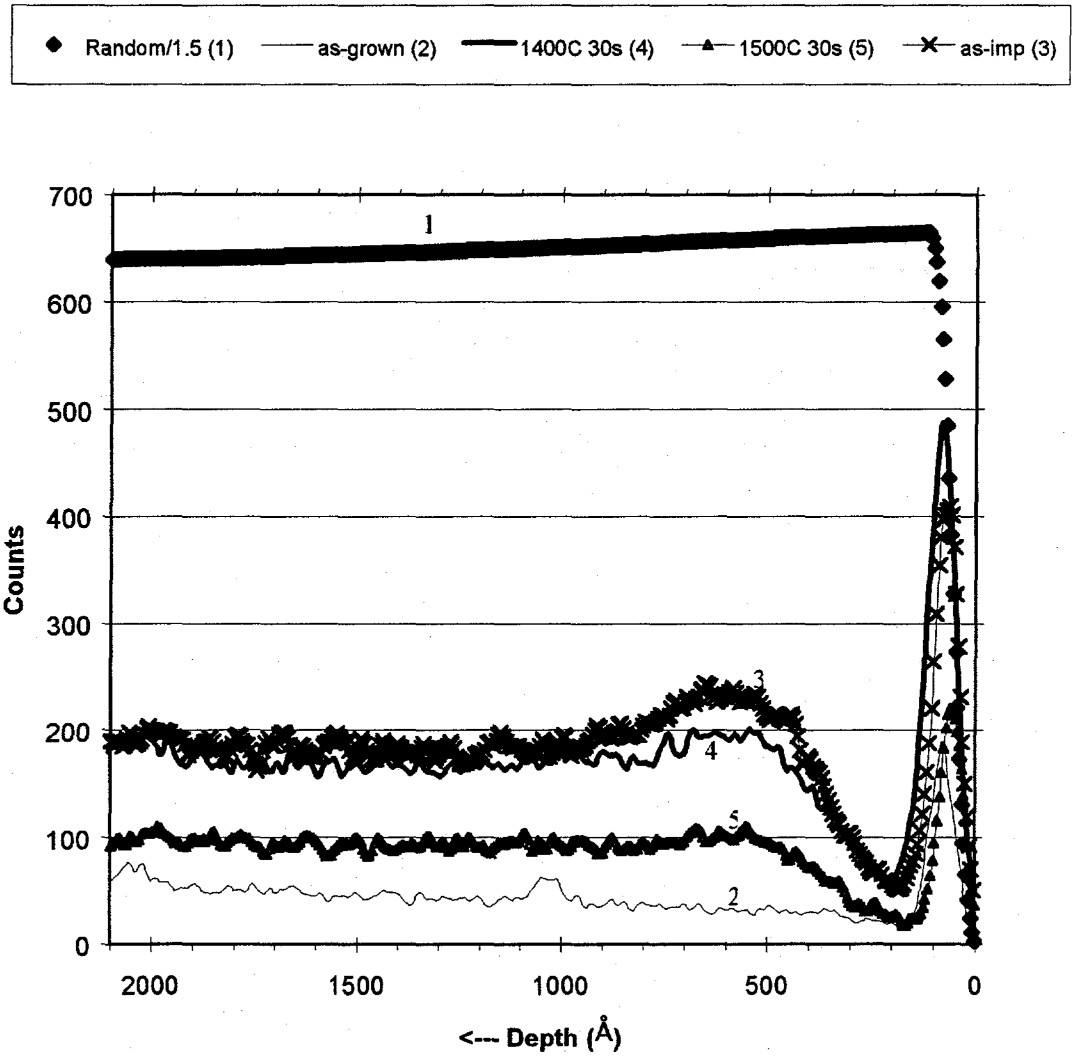

Figure 3.4. 1.92 MeV He^+ <0001> aligned RBS spectra of GaN layers implanted with As (10^{15} cm^{-2}) and Be (10^{15} cm^{-2}) with different annealing treatments.

Damage recovery in samples implanted with both As and Ga is shown in figure 3.5. Annealing was performed at 1400°C for 30s and 60s. The change in time was not expected to generate a significant difference in damage recovery as compared to a change in temperature because damage recovery is a thermally activated process with a strong exponential dependence given by $\exp\left[\frac{-E_A}{kT}\right]$. It is apparent though that there is considerably more damage recovery after 60s. One possible explanation is that the sample did not reach the full annealing temperature in a time short compared to the 30s annealing. In this case the sample was not at 1400°C for any significant amount of time. We observe that after annealing at 1400°C for 60s, less than half as many displaced Ga atoms remain as compared to the sample annealed at 1400°C for 30s. The depth of damage is reduced after annealing at 1400°C for 30s from ~1100 Å to ~1000 Å, and it is further reduced to ~900 Å after annealing at 1400°C for 60s.

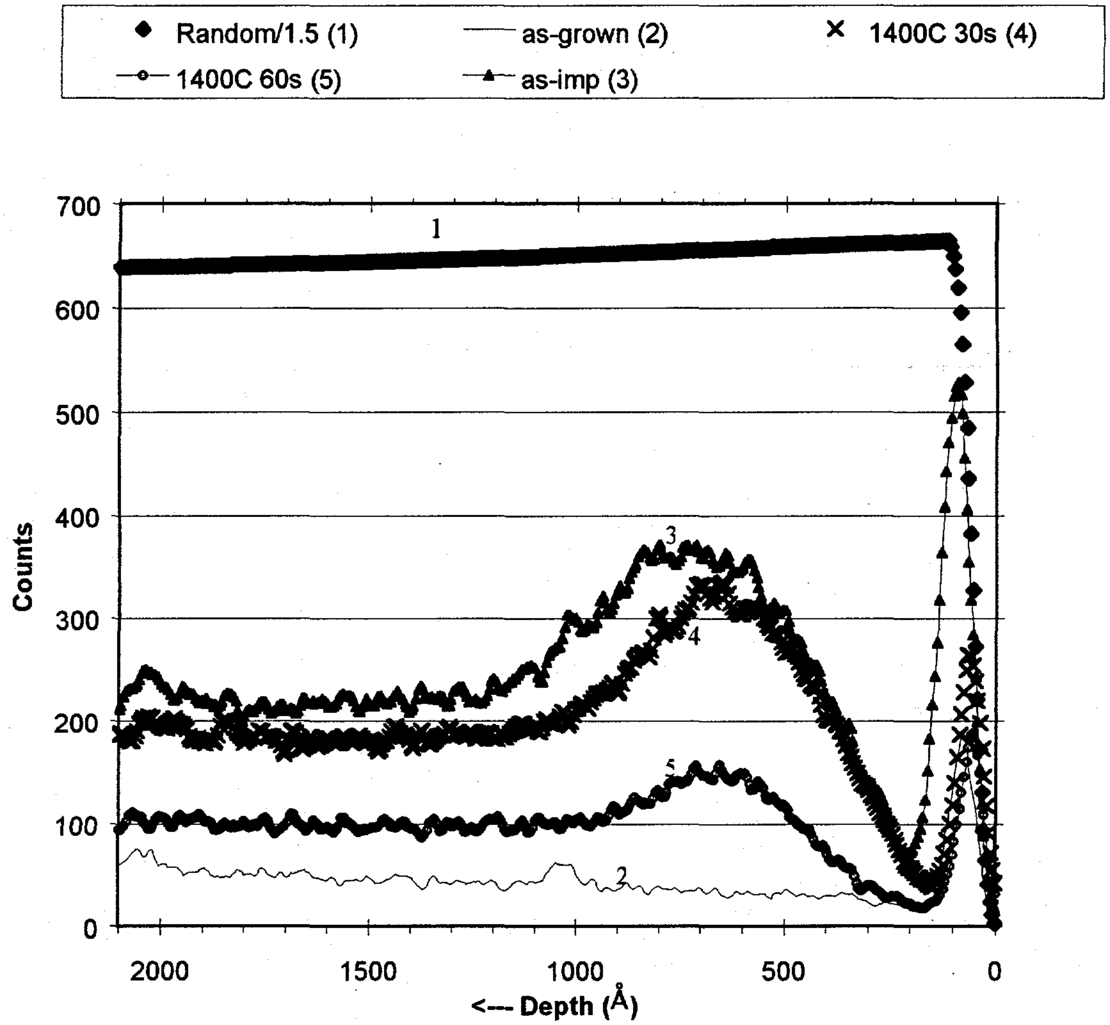

Figure 3.5. 1.92 MeV He^+ <0001> aligned RBS spectra of GaN layers implanted with As (10^{15} cm^{-2}) and Ga (10^{15} cm^{-2}) with different annealing treatments.

3.2 Implantation and annealing effects

Be was implanted to volume concentrations of $\sim10^{19}$cm^{-3} to $\sim10^{20}$ cm^{-3} and co-implanted with As at an energy which led to similar concentration profiles for Be and As. As was chosen as the co-implant species to optimize damage effects and retain III-V stoichiometry of the crystal. Some samples were implanted with just As to separate the effects of As from results obtained from the samples implanted with both As and Be. Photoluminescence was performed on the as-implanted, the as-grown and the annealed samples to determine if optically active levels were introduced by the implanted impurities.

Samples were too resistive after implantation, and even after annealing to perform accurate Hall effect and resistivity measurements. Sample resistances measured with an ohmmeter across evaporated contacts were found to be on the order of >10 MΩ. Hall effect results obtained were determined to be inaccurate because the results were extremely inconsistent between different measurement runs on the same sample. As shown in the previous section, damage still remains in the samples even after annealing at 1500°C, and the residual damage is probably why the samples remain so highly resistive.

3.2.1 Published work on Be and As in GaN

Be has been investigated previously as an alternative acceptor in GaN. Nearly all studies have only reported PL data in their work and used the PL results to assign Be optical activation energies.

As far back as 1976, Pankove and Hutchby implanted numerous elements individually into GaN films, thermally annealed them and measured PL. PL spectra of

Be implanted films showed only a broad emission at ~2.16 eV. This was similar to previous results which also showed a broad luminescence band centered at about ~2.2 eV after implantation of Be (Ilegems and Dingle, 1973). More recently, another group (Ronning et al., 1998), implanted Be as well as Be co-implanted with nitrogen into GaN films. After annealing at 600°C and 900°C, a weak new luminescence at 3.35 eV appeared which they attributed to recombination from the conduction band to Be acceptors. From this assignment, they proposed an optical activation energy for Be acceptors of ~150 meV. The co-implantation with N did not improve their results. However, this is not surprising because N is another light element, and it is not expected to create significantly more damage to improve the substitution of Be on Ga sites.

Other experimenters doped the GaN films with Be during MBE growth. Features in the PL spectrum between 2.95 and 3.18 eV were reported, and Be acceptor states at E_v + 250 meV were proposed (Salvador et al., 1996). PL emission at these energies is common for Mg-doped GaN, and the energy level predicted for Be-doped GaN from peak emissions between 2.95 and 3.18 eV is similar to energies predicted from PL data for Mg-doped GaN. Two other groups reported new PL emissions after MBE growth of Be-doped GaN. One group reported a new emission at 3.385 eV as well as 1st and 2nd phonon replica lines (Dewsnip et al., 1998), and the second group reported a new emission at 3.384 eV (Sanchez et al., 1998) which is comparable to the 3.385 eV reported by Dewsnip et al. Both attributed the new emissions to residual donor to Be acceptor transitions and assigned an optical ionization energy of ~90-100 meV to the Be acceptors.

It is expected that an isovalent impurity such as As in GaN would not create levels in the bandgap. However, in studies of As in GaN made previously, PL data as well as theoretical predictions about the behavior of As in the GaN bandgap indicate that As indeed forms deep levels in the bandgap. As was also one of the many elements implanted in GaN by Pankove and Hutchby (Pankove and Hutchby, 1976). Implanted As generated distinct new PL emissions at 2.58 eV. This As-related emission was repeated in other As-implanted GaN studies with similar emissions at 2.6 eV and 2.597 eV reported (Li et al., 1990; Jadwisienczak and Lozykowski, 1998). Theoretically, As is predicted to form a deep state in the GaN bandgap (Mattila and Zunger, 1998). However, the calculated level of $E_v + 0.75$ eV differs significantly from experimental results; this value would correspond to PL emission at ~2.75 eV, far from any values reported by the various experimenters.

3.2.2 Effects of As and Be implantation

A PL spectrum of the as-grown p-GaN material was taken as a reference and is shown in figure 3.6. The main feature in this spectrum is the Mg-related emission at ~3.05 eV (M). A high resolution measurement was made of the 3.3 – 3.5 eV range and is shown in figure 3.7. It is worthwhile to note that spectral features at 3.357 eV (C), 3.431 eV (B) and 3.448 eV (A) are present in the as-grown material. Peak A is the acceptor bound exciton peak (AX) and peak C is its phonon replica lying 91 meV lower in energy from peak A. The origins of peak B are undetermined, however it may be another AX with the exciton bound to an acceptor of larger binding energy.

PL of As implanted and annealed films are shown in figures 3.8 – 3.11. There are two broad peak emissions that dominate all the spectra. The higher energy peak is believed to be the Mg-related emission (M) that is present in the as-grown p-GaN spectrum. The lower energy peak (L) then is either related to As or to implantation damage. With increased annealing temperatures both peaks gradually shift to lower energies. Throughout the annealing stages from as-implanted to annealing at 1400°C for 30s, the Mg-related emission is stronger relative to the lower energy peak, peak L. However, after annealing at 1500°C for 30s, the low energy peak increases dramatically relative to the Mg-related peak as shown in figure 3.11. Since disorder in the crystal is significantly reduced from annealing at 1400°C to 1500°C as evidenced in the c-RBS data shown previously in figure 3.2, it is likely that this broad emission is related to As and not damage. However, Ga- vacancies acting as deep acceptors and V_{Ga}-donor complexes have been attributed to the formation of the yellow luminescence emission at ~2.2eV (Van de Walle and Neugebauer, 1997). Ga vacancies must have formed in our samples during As implantation. After annealing at 1500°C, SIMS measurements showed that oxygen diffused into the layer possibly forming V_{Ga}-O complexes as well. Therefore, the large PL feature centered around 2.3 eV could, in principle, be due to V_{Ga}-O complexes. To obtain a unique assignment of this PL peak noble gas implants should be studied.

Figure 3.9 shows the PL spectrum of an as implanted sample which was annealed at 900°C for 10 minutes. Only in this spectrum do spectral features besides peaks L, M, A, B and C emerge. These new features emerge between 3.0 and 3.4 eV, and the most intense feature labeled G in the plot may be due to recombinations between donor levels and the valence band. The smaller features in this range are more difficult to discern and remain unknown.

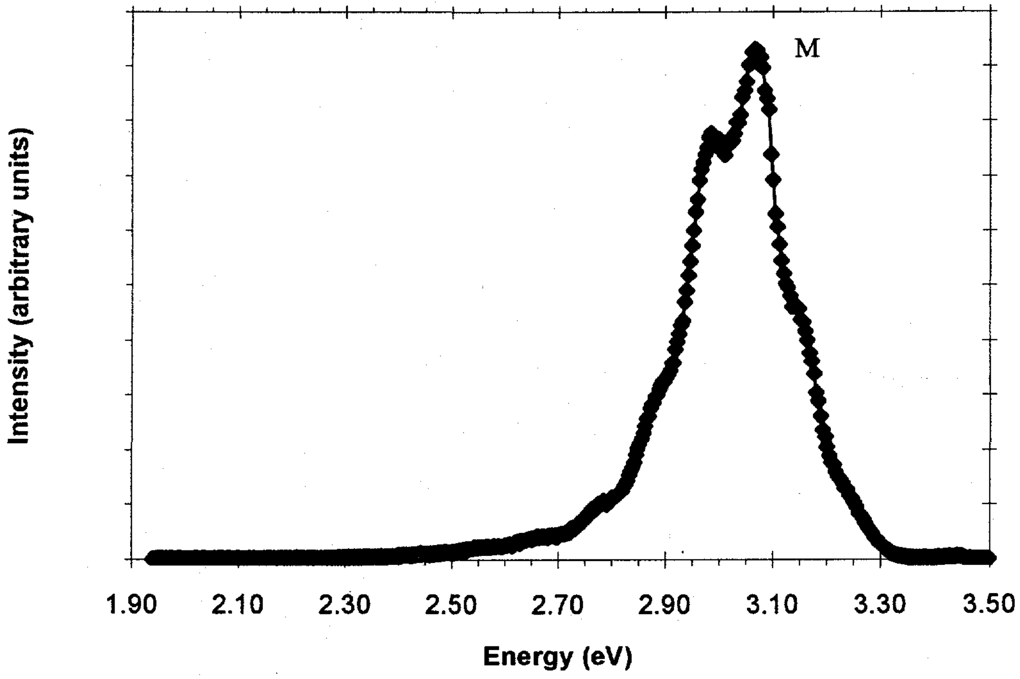

Figure 3.6. 12K PL spectrum of as-grown p-type GaN:Mg.

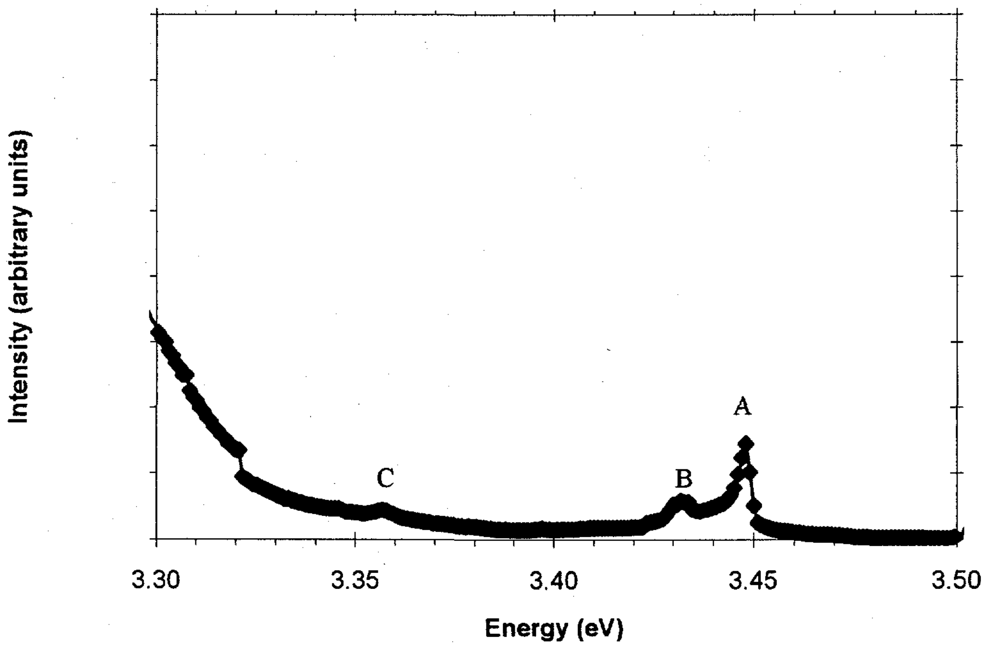

Figure 3.7. Detail of the 12K PL spectrum in the 3.3 –3.5 eV range of as-grown p-type GaN:Mg.

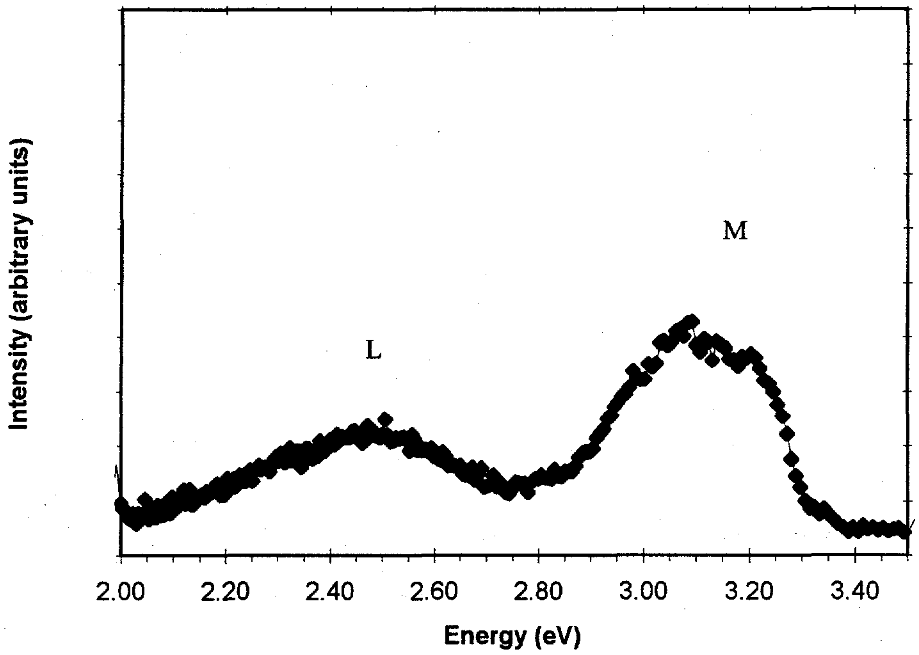

Figure 3.8. 12K PL spectrum of p-type GaN:Mg implanted with As.

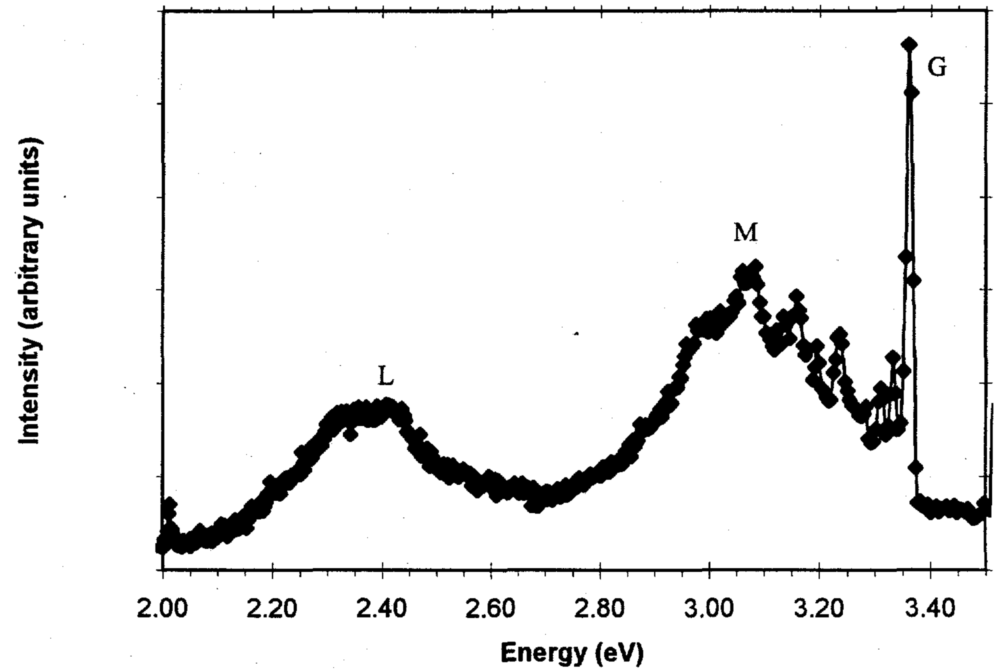

Figure 3.9. 12K PL spectrum of p-type GaN:Mg implanted with As and annealed at 900°C for 10 minutes.

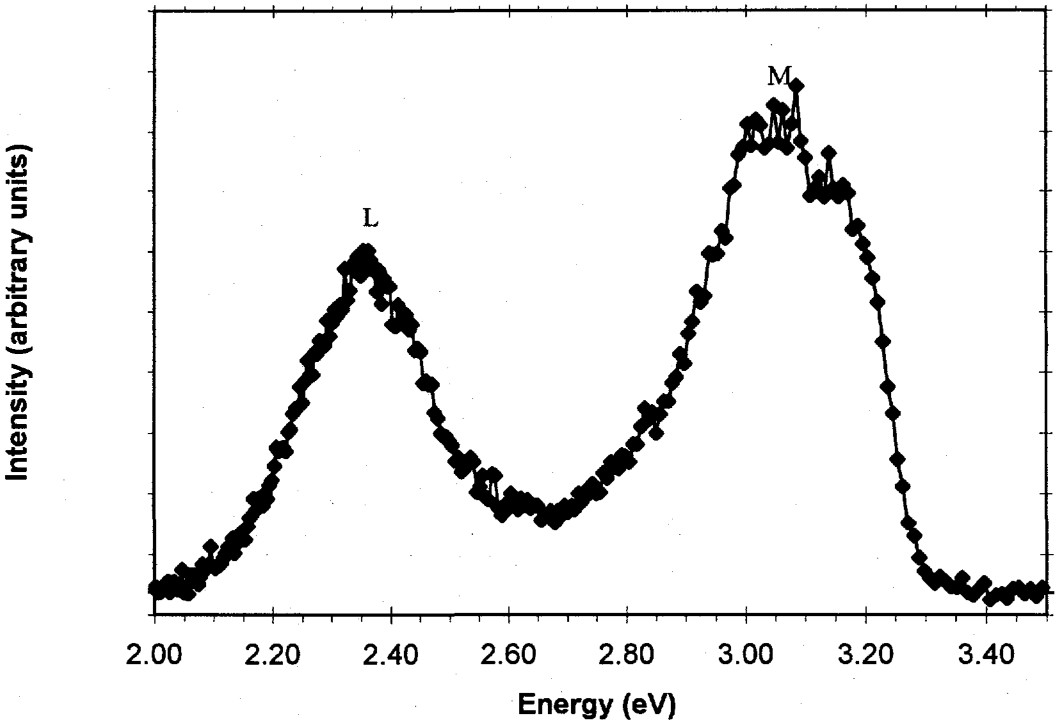

Figure 3.10a. 12K PL spectra of p-type GaN:Mg implanted with As and annealed at 1400°C for 30s.

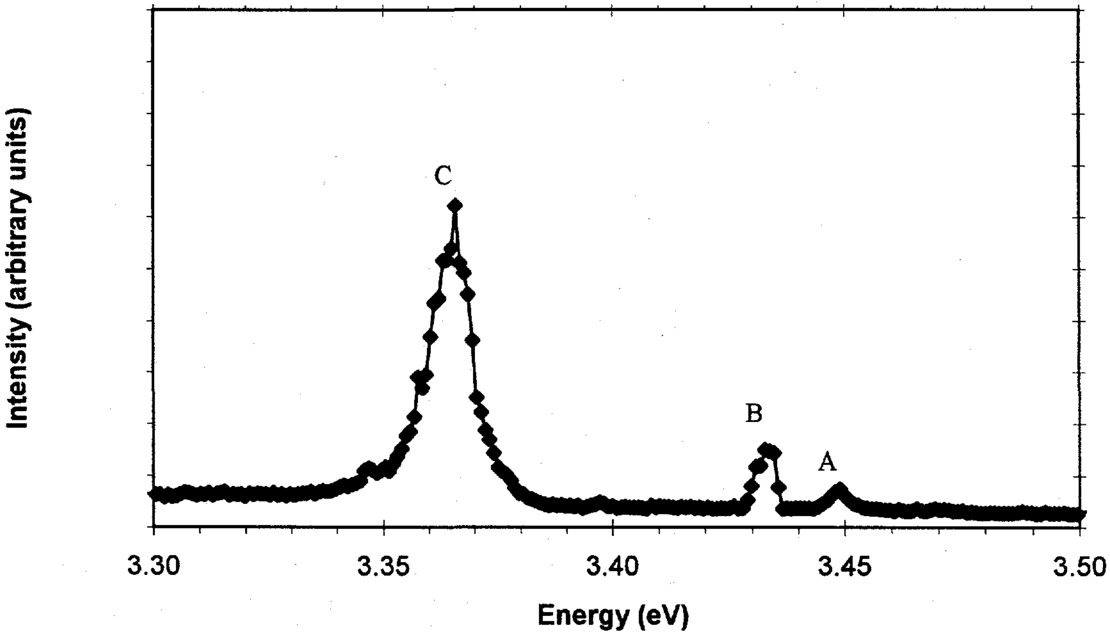

Figure 3.10b. Detail of the 12K PL spectrum between 3.3 and 3.5 eV of p-type GaN:Mg implanted with As and annealed at 1400°C for 30s.

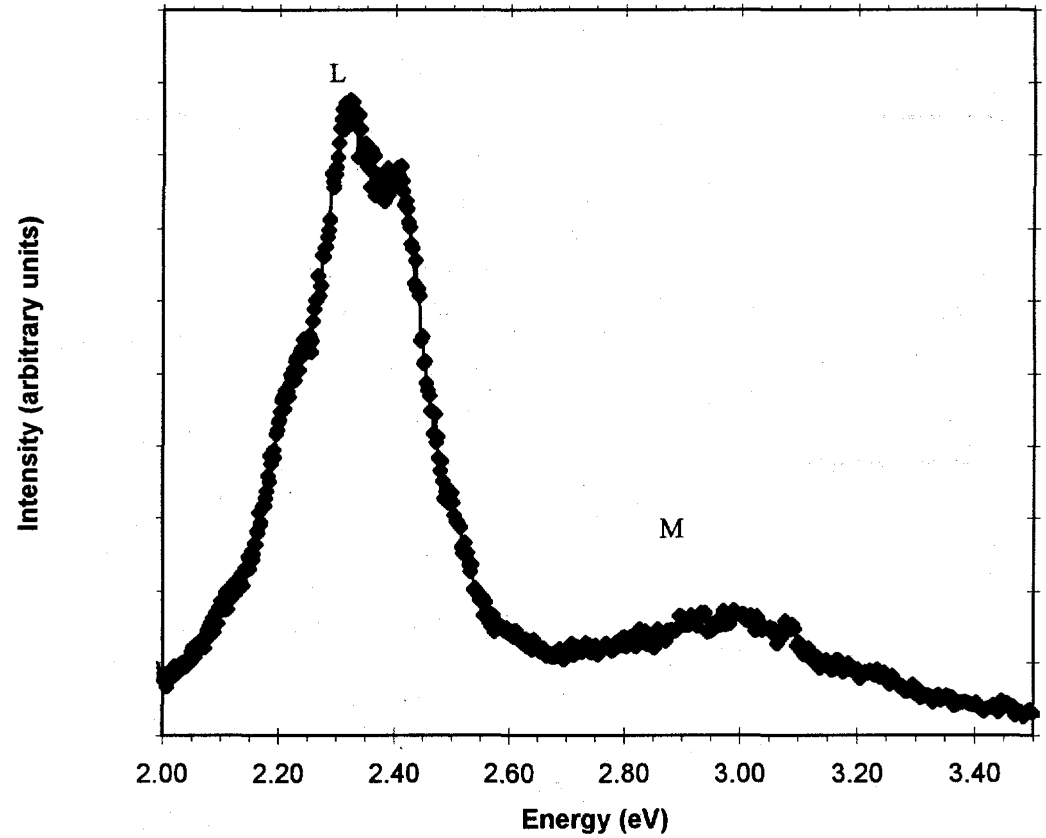

Figure 3.11. 12K PL spectrum of p-type GaN:Mg implanted with As and annealed at 1500°C for 30s.

PL spectra of GaN implanted with As and Be are shown in figures 3.12 – 3.17. No new peaks arise with the addition of Be implantation. Looking at the 3.3-3.5 eV range in more detail, only peaks A, B and C at 3.448 eV, 3.342 eV and 3.357 eV which were present in the as-grown material. In figure 3.14b a new peak at 3.487 eV (D) emerges, however this peak is related to the donor bound exciton DX. The other small peaks labeled E, F and G on the plot are believed to be plasma lines which have appeared in other PL spectra measured by this system. Again though, the trend with increased annealing temperature and increased damage recovery as shown from c-RBS spectrum, is an increase in the low energy peak centered about ~2.3 eV relative to the Mg-related peak.

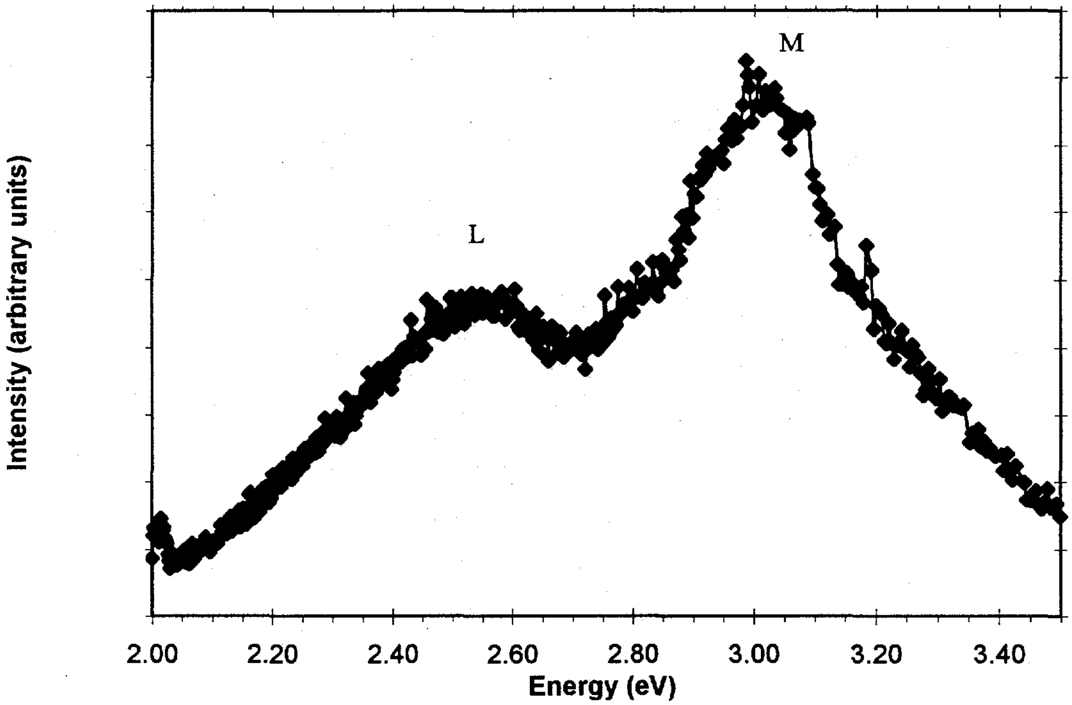

Figure 3.12. 12K PL spectrum of p-type GaN:Mg as-implanted with As and Be (10^{14} cm^{-2}).

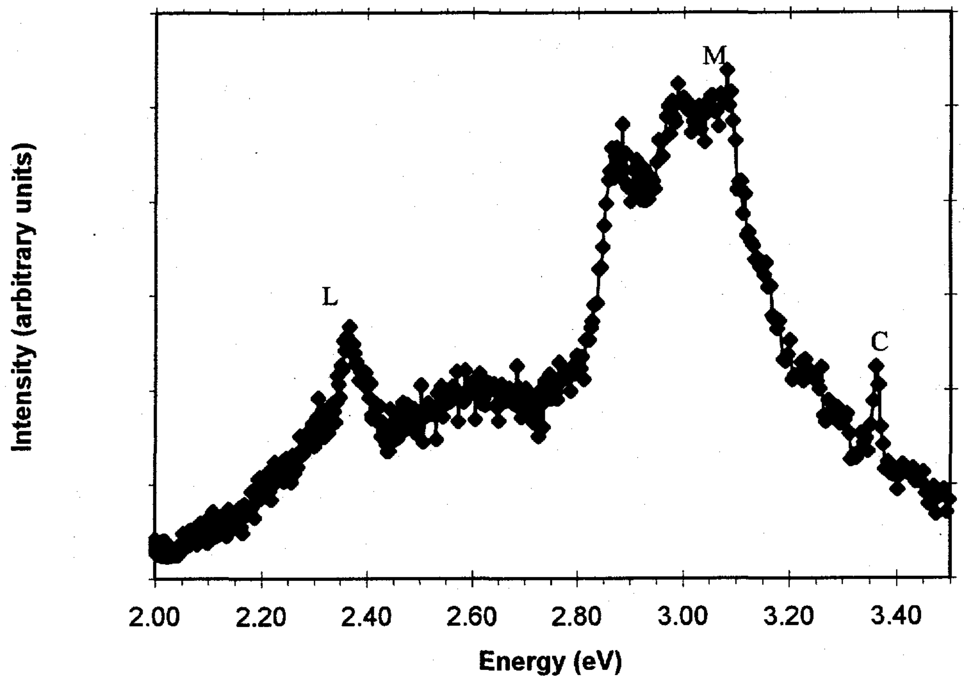

Figure 3.13a. 12K PL spectrum of p-type GaN:Mg implanted with As and Be (10^{14} cm^{-2}); annealed at 900°C for 10 minutes.

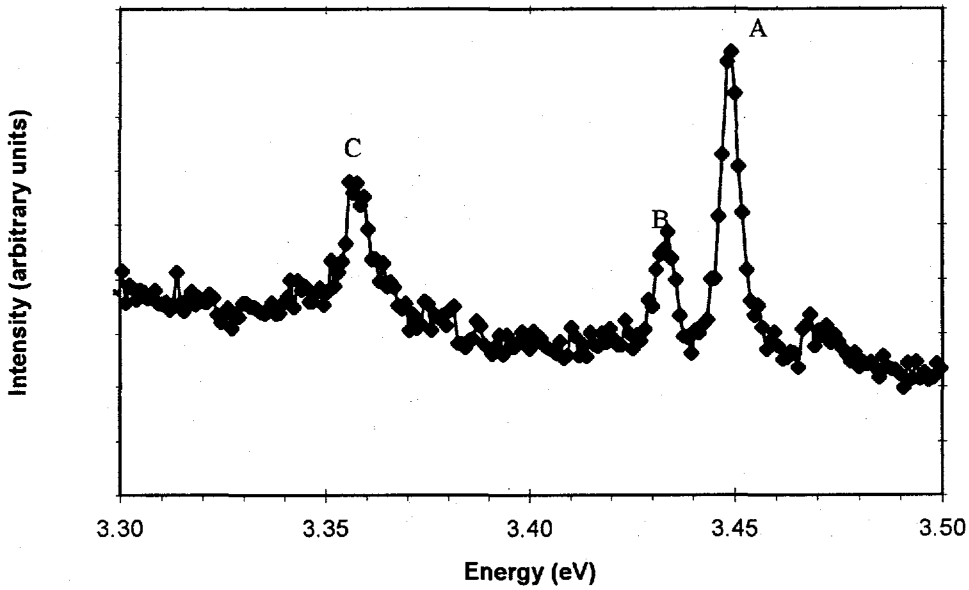

Figure 3.13b. Detail of the 12K spectrum between 3.3 and 3.5 eV of p-type GaN:Mg implanted with As and Be (10^{14} cm^{-2}); annealed at 900°C for 10 minutes.

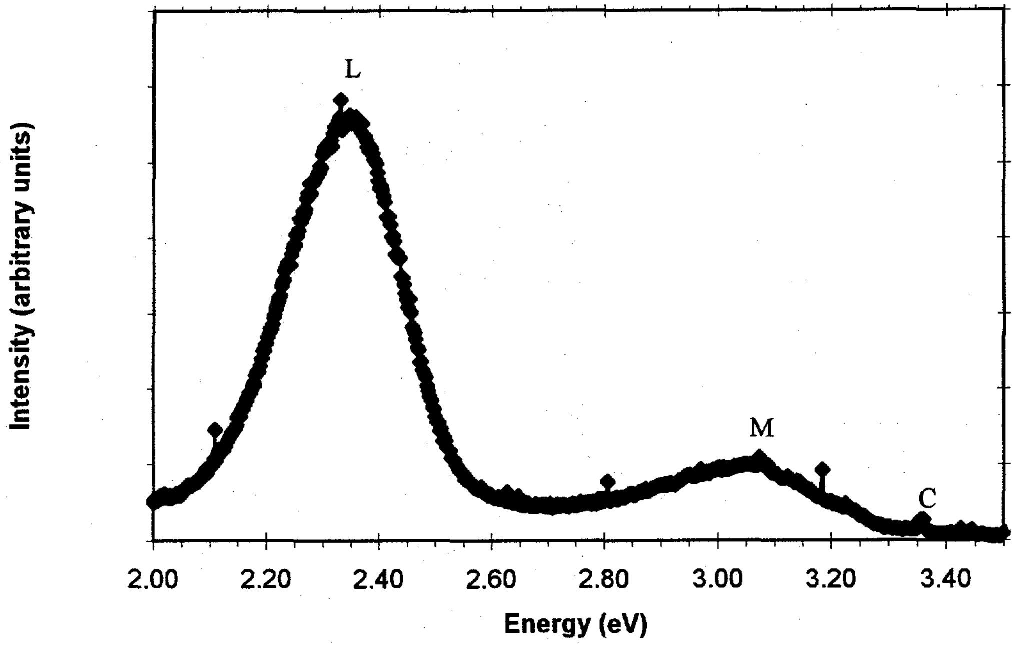

Figure 3.14a. 12K PL spectrum of p-type GaN:Mg implanted with As and Be (10^{14} cm^{-2}); annealed at 1400°C for 30s.

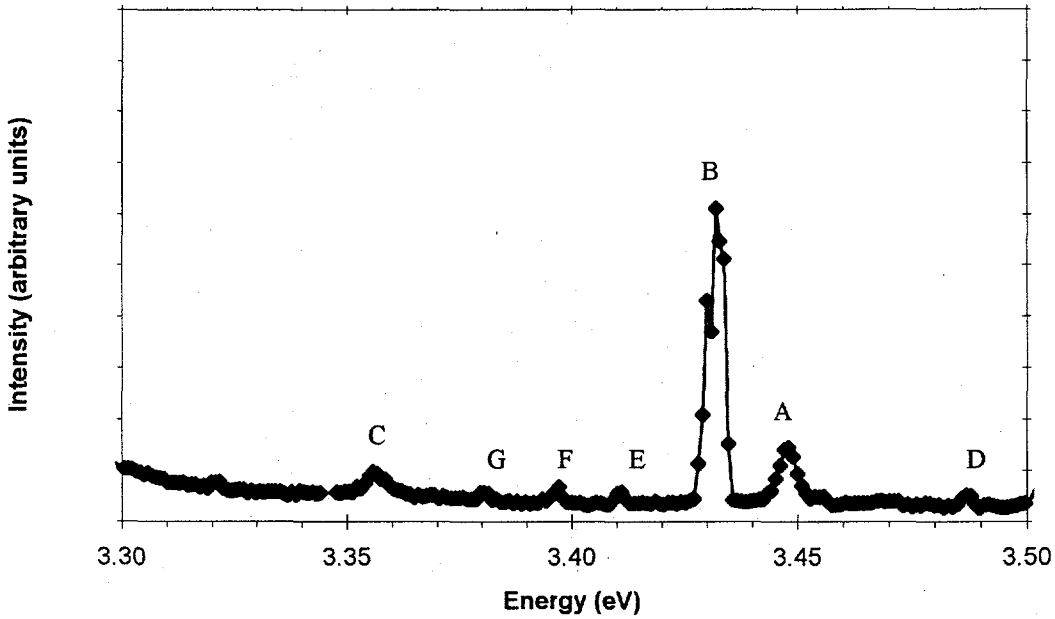

Figure 3.14b. Detail of the 12K PL spectrum between 3.3 and 3.5 eV of p-type GaN:Mg implanted with As and Be (10^{14} cm^{-2}); annealed at 1400°C for 30s.

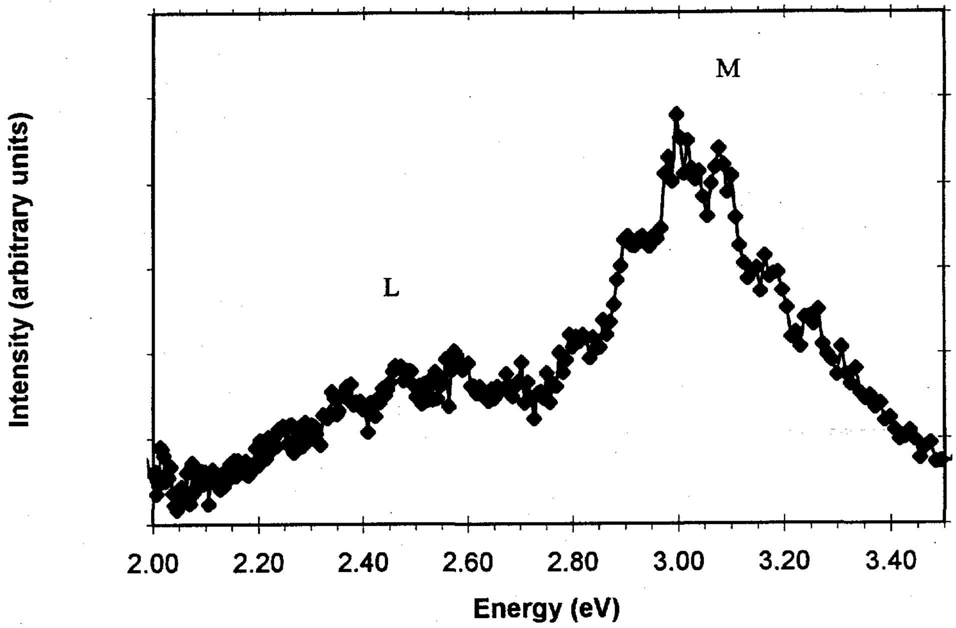

Figure 3.15. 12K PL spectrum of p-type GaN:Mg implanted with As and Be (10^{15} cm^{-2}); no annealing.

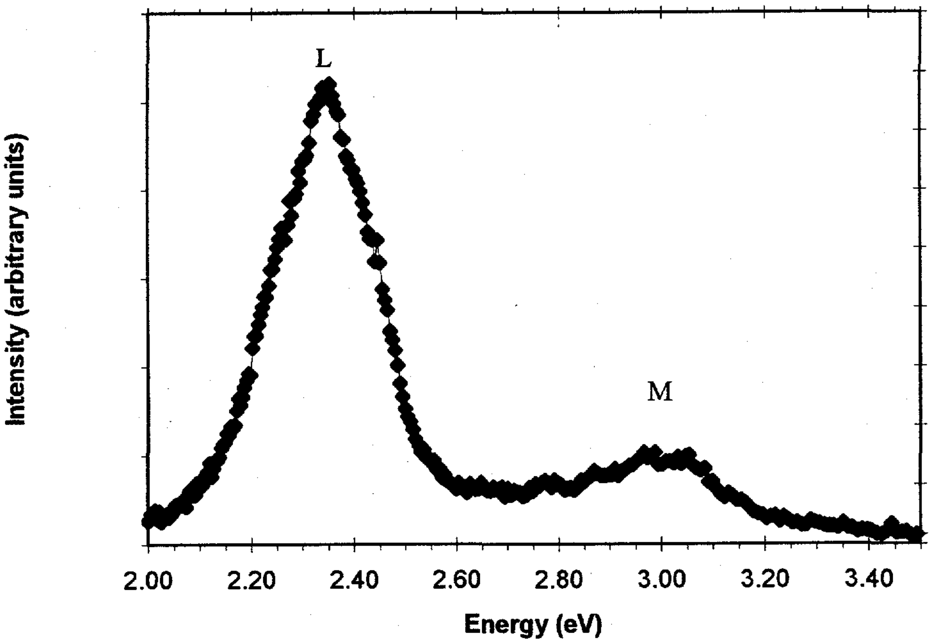

Figure 3.16. 12K PL spectrum of p-type GaN:Mg implanted with As and Be (10^{15} cm^{-2}); annealed at 1400°C for 30s.

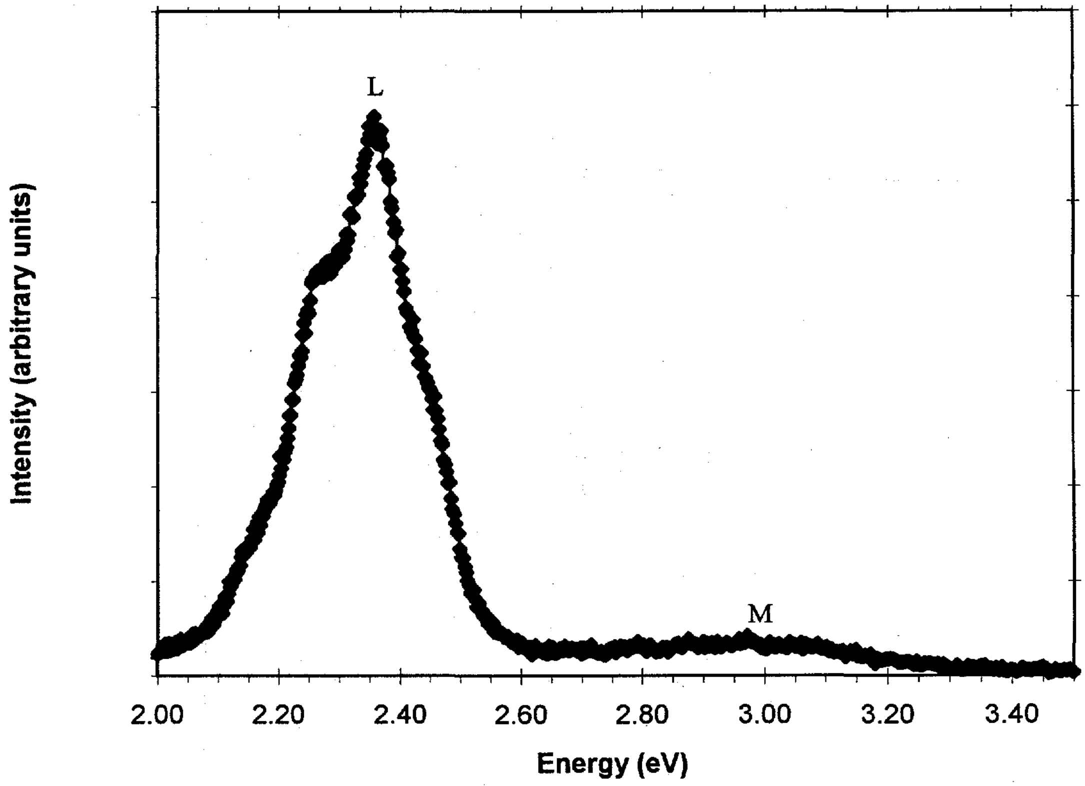

Figure 3.17. 12K PL spectrum of p-type GaN:Mg implanted with As and Be (10^{15} cm^{-2}); annealed at 1500°C for 30s.

3.3 Hydrogenation of Be implanted p-GaN

In previous studies, Brandt et al. (1994) reported diffusion of hydrogen (deuterium) from a plasma into p-type GaN. Their studies showed by SIMS that hydrogen does in fact diffuse into the layer, and that it reduces the free hole concentration suggesting the formation of Mg-H complexes. Preliminary experiments adding hydrogen to As and Be implanted GaN films were made in our studies. Two samples implanted with As and Be (10^{15} cm^{-2}) were hydrogenated at different points in their processing steps. The first sample was exposed to the hydrogen plasma at 600°C for 1 hour directly following implantation. The implanted and hydrogenated sample was then capped with an AlN layer and annealed at 1500°C for 30s. After annealing the cap was removed in hot KOH and the sample was subjected to the thermal annealing cycle that is normally used to activate Mg by H-removal: 750°C for 10 minutes. PL was measured post-hydrogenation but pre-annealing, as shown in figure 3.18. Because no implanted film had been annealed at 600°C for 1 hour previously, there was no PL spectrum of a non-hydrogenated similar film to compare this to. However, the spectrum displays an intermediary stage of the sample between the as-implanted film (figure 3.15) and the film annealed at 900°C for 10 minutes (figure 3.20). After the high temperature annealing, the PL spectrum, shown in figure 3.19, is equivalent to the PL spectrum of the sample annealed at 1500°C for 30s that was not exposed to the hydrogen plasma (figure 3.17).

The second sample was exposed to the hydrogen plasma following an initial annealing step at 900°C for 10 minutes. PL of the sample after annealing at 900°C for 10 minutes as shown in figure 3.20. Following hydrogenation, this sample was also capped, annealed at 1500°C for 30s, uncapped and subjected to an activation annealing at 750°C for 10 minutes. PL was measured after the final processing step, as shown in figure 3.21. Again, no new PL peaks were detected; the spectrum was nearly equivalent to previous spectra of films implanted and then annealed at 1500°C for 30s.

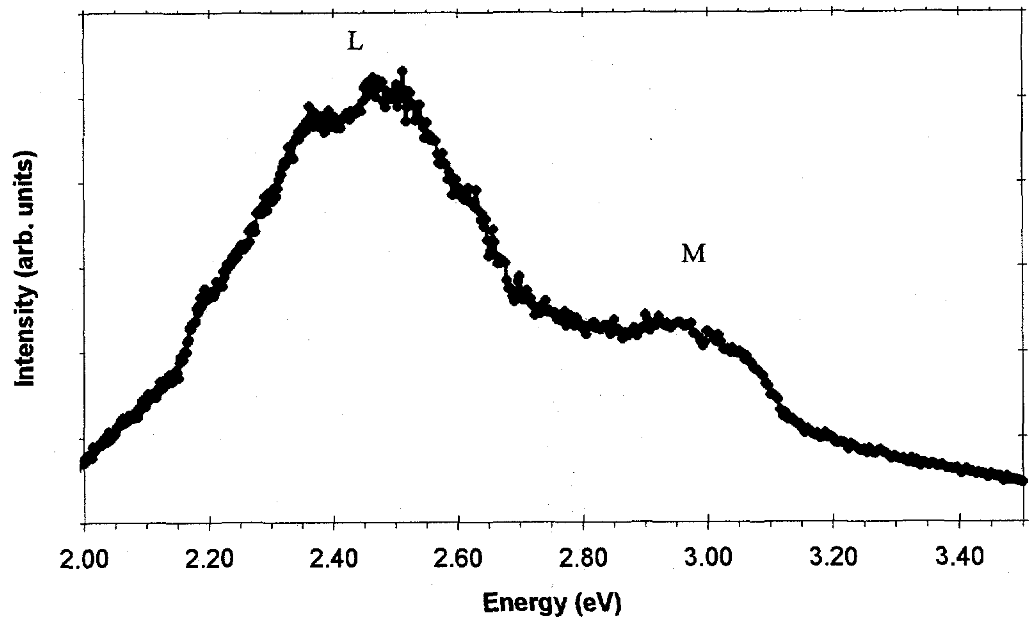

Figure 3.18. 12K PL spectrum of p-type GaN:Mg implanted with As and Be, hydrogenated at 600°C for 1 hour.

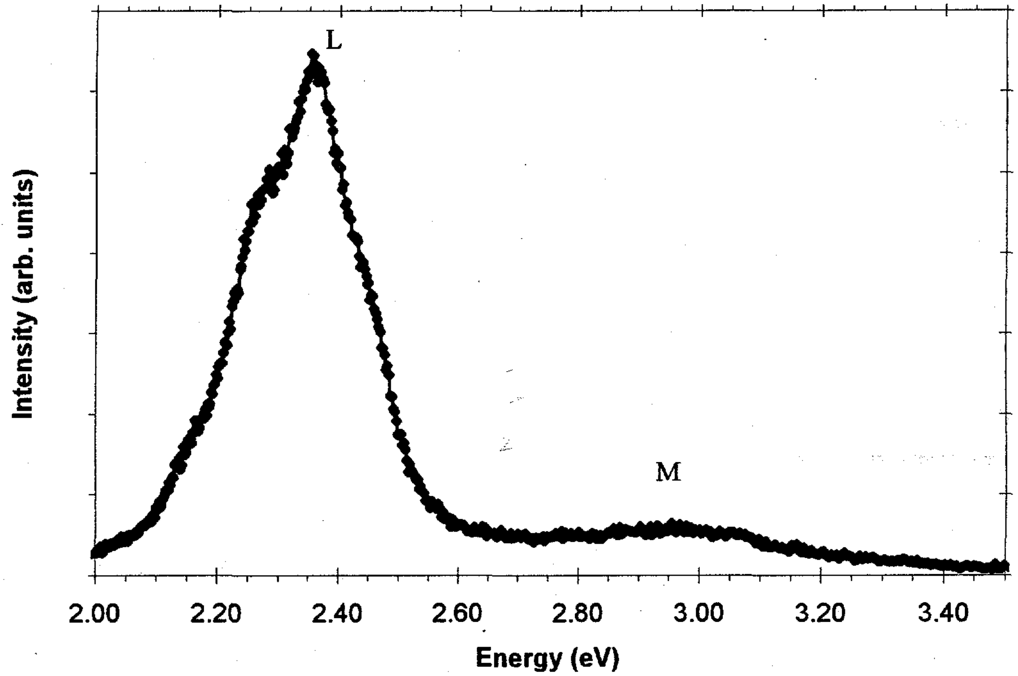

Figure 3.19. 12K PL spectrum of p-type GaN:Mg implanted with As and Be, hydrogenated at 600°C for 1 hour and annealed at 1500°C for 30s.

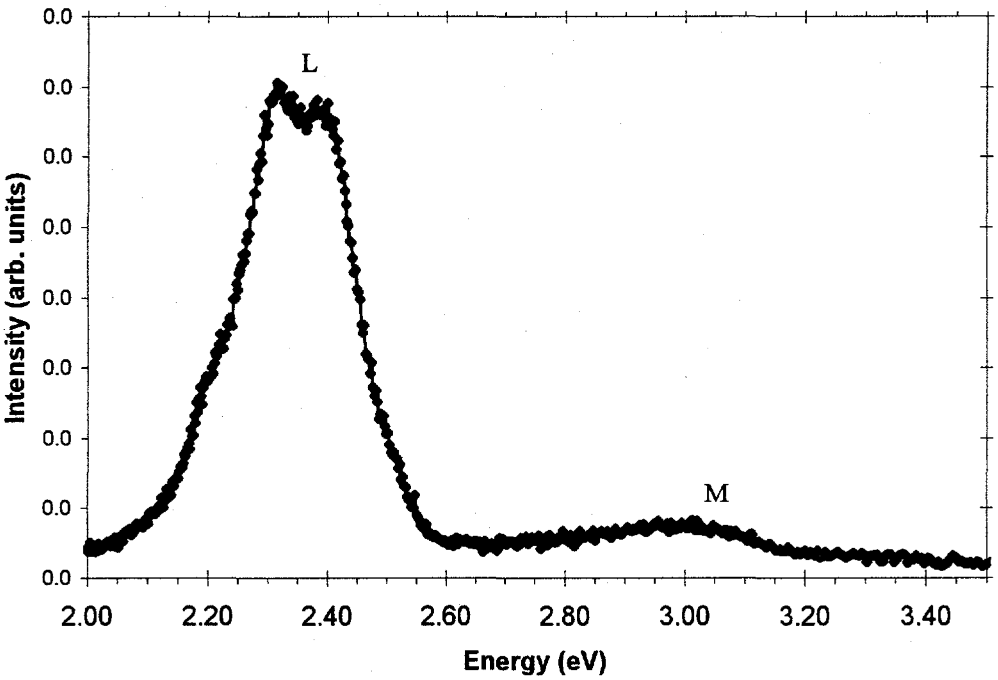

Figure 3.20. 12K PL spectrum of p-type GaN:Mg implanted with As and Be, annealed at 900°C for 10 minutes.

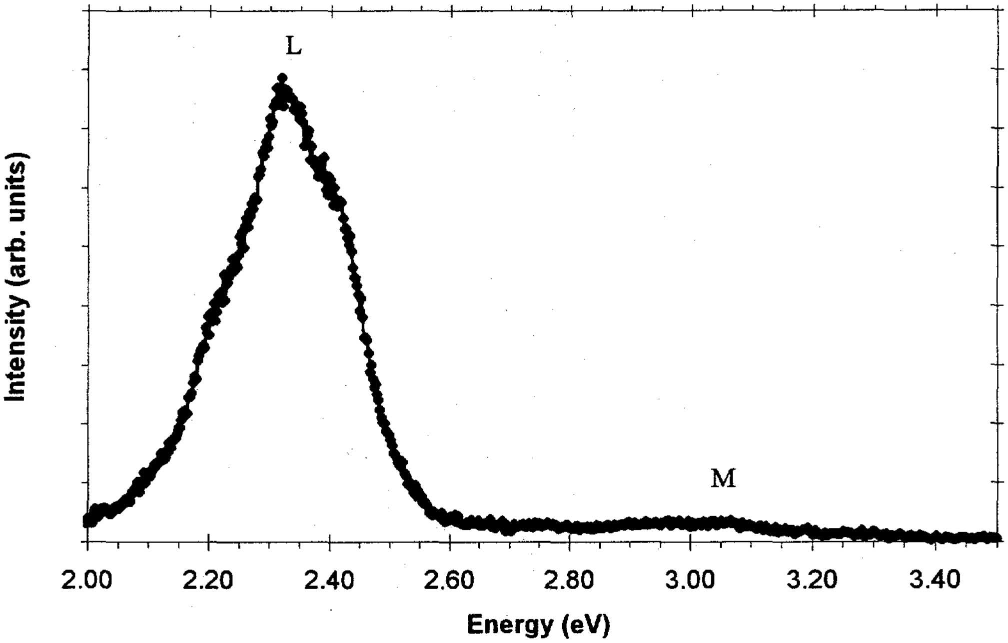

Figure 3.21. 12K PL spectrum of p-type GaN:Mg implanted with As and Be, annealed at 900°C for 10 minutes, hydrogenated at 600°C for 1hour, and annealed at 1500°C for 30s.

To determine if H was indeed introduced into the sample, several samples were specifically prepared for SIMS analysis by exposure to a deuterium plasma. Deuterium was introduced into the hydrogenation system, and three samples were processed according to the steps shown in table 3.1.

Sample	Processing Step 1	Processing Step 2	Processing Step 3
2	Implant	Deuterate at 600°C for 1 hour	
3	Implant	Anneal at 1500°C for 30s	Deuterate at 600°C for 1 hour
4	Implant	Anneal at 1500°C for 30s	Deuterate at 600°C for 2 hours

Table 3.1. Processing steps for samples exposed to deuterium plasma.

It is apparent from figures 3.22, 3.23 and 3.24 that ^2H was introduced into the GaN film. The dotted line in each of the plots represents the calculated concentrations of ^1H, which need to be present if the ^2H concentration in the film occured naturally. In all cases, the calculated concentration was greater than the measured concentration of ^1H. Therefore we know that ^2H from the plasma diffused into the layer. However, we also note that ^2H did not penetrate further that ~300Å under any processing condition.

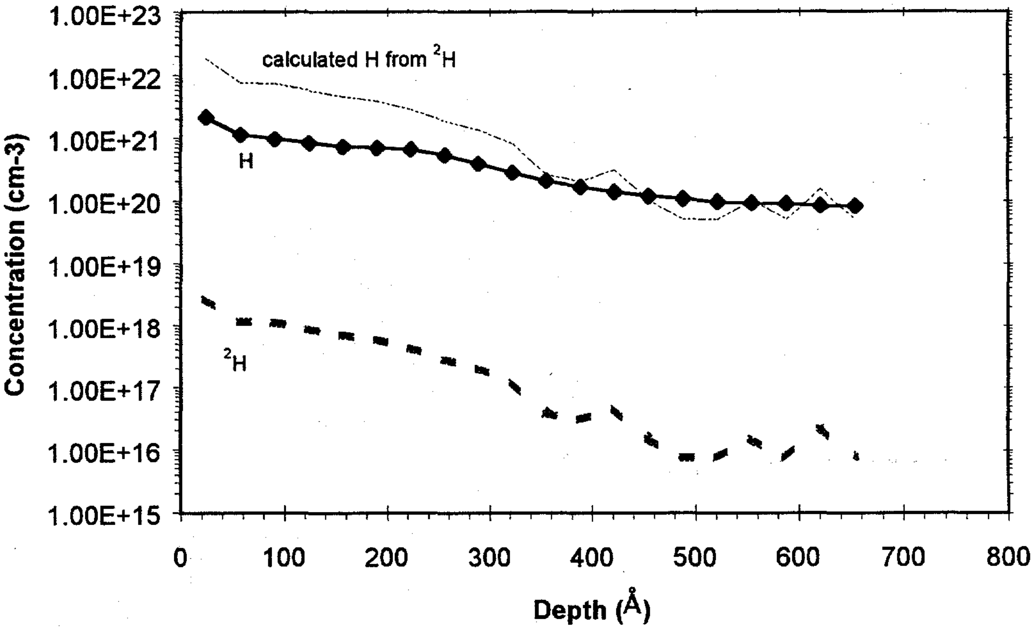

Figure 3.22. Measured ^{1}H, ^{2}H and calculated ^{1}H SIMS depth profiles of a As + Be implanted p-type GaN:Mg film exposed to deuterium plasma at 600°C for 1 hour.

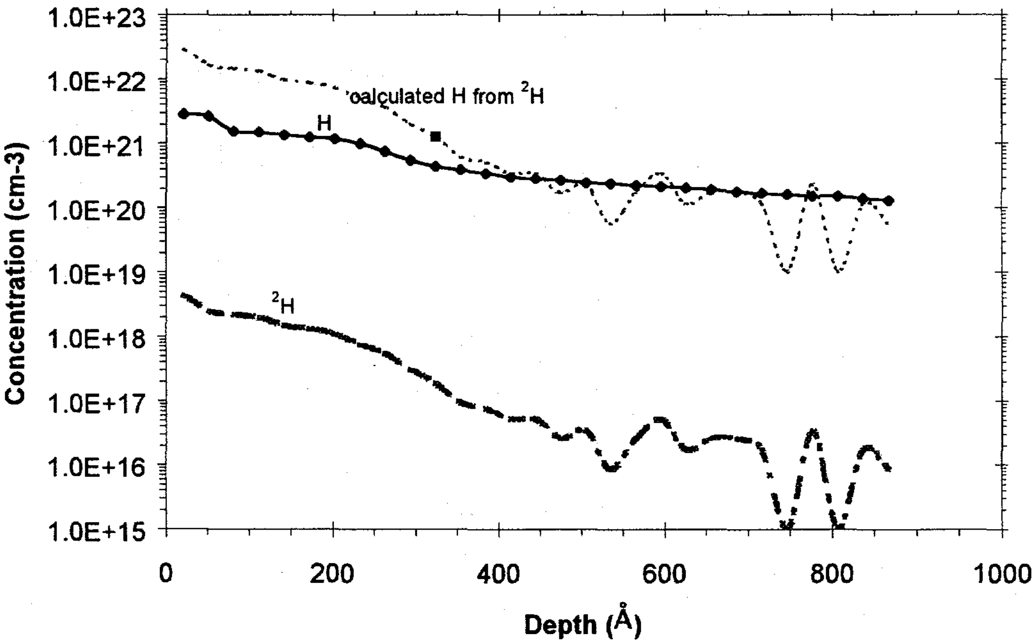

Figure 3.23. Measured ^{1}H, ^{2}H and calculated ^{1}H SIMS depth profiles of a As + Be implanted p-type GaN:Mg film exposed to deuterium plasma at 600°C for 1 hour after annealing at 1500°C for 30s.

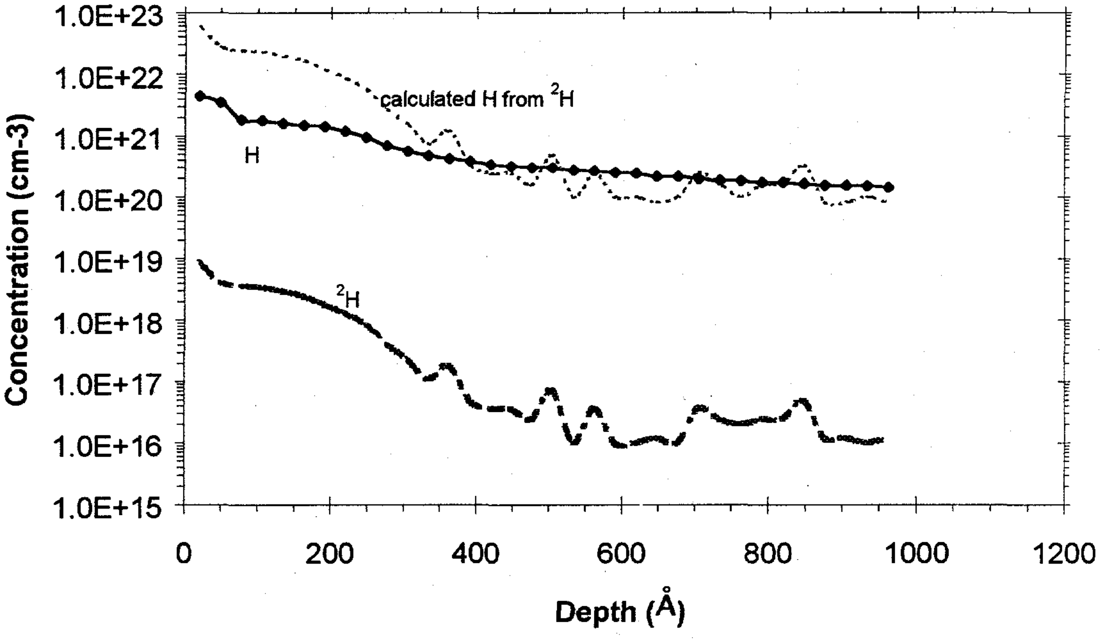

Figure 3.24. Measured ^{1}H, ^{2}H and calculated ^{1}H SIMS depth profiles of a p-type GaN:Mg film exposed to deuterium plasma at 600°C for 2 hours after an annealing at 1500°C for 30s.

Sample 4 was exposed to the deuterium plasma twice as long as sample 3, and one would expect that the ^{2}H incorporation to increase in concentration, unless limited by solubility, and have a deeper diffusion tail in the sample that was exposed for twice the time. Both ^{2}H concentrations and ^{1}H concentrations for samples 3 and 4 were plotted together in figure 3.25. The concentration of ^{2}H in sample 4 was two times the concentration of ^{2}H in sample 3, with a surface concentration of 8.6×10^{18} cm^{-3} as compared to 4.4×10^{18} cm^{-3}. However, ^{2}H penetrated to only ~300Å in both cases. It appears as if the ^{2}H piled up at the surface. This could be caused by the trapping of ^{2}H at defects remaining in the near surface of the crystal.

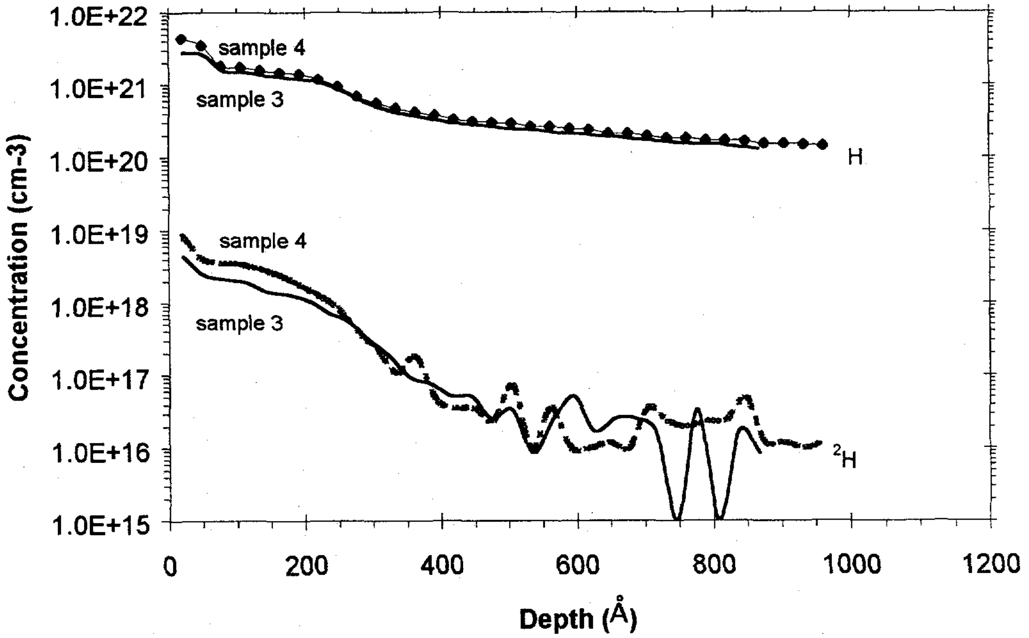

Figure 3.25. SIMS depth profiles of measured ^{1}H and ^{2}H in samples exposed to the deuterium plasma for 1 hour and 2 hours each.

3.4 Diffusion of oxygen from the capping layer and the substrate into the GaN film

Oxygen is a deep level donor impurity in GaN residing in the conduction band. It contributes to n-type conduction. Oxygen contamination by diffusion into the p-GaN layers during annealing was a concern, because oxygen atoms acting as donors may compensate and overshadow any effects sought by introducing potential acceptors into the semiconductor. It is possible that oxygen was introduced during two different processing steps. During implantation, oxygen on the surface may have been “knocked” in by the ions projected into the layer. Secondly, oxygen may have diffused from the AlN cap or from the substrate into the GaN layer during annealing. The sputtered AlN capping layers which were used to prevent the GaN films from decomposing during high temperature annealing were found to contain a significant amount of oxygen. From simulations made to replicate the obtained RBS spectrum of sputtered AlN films, oxygen incorporation in the AlN layers was determined to be no greater than 10% for the sputter conditions used.

By SIMS analysis, oxygen depth profiles were determined for GaN films before and after implantation and annealing with an AlN cap. The oxygen profiles for the as-grown and as-implanted samples are shown in figure 3.26. From the data taken, it did not appear as if oxygen was knocked into the sample surface by implantation. All of the profiles for the implanted samples showed oxygen surface profiles that were steeper than the as-grown control sample.

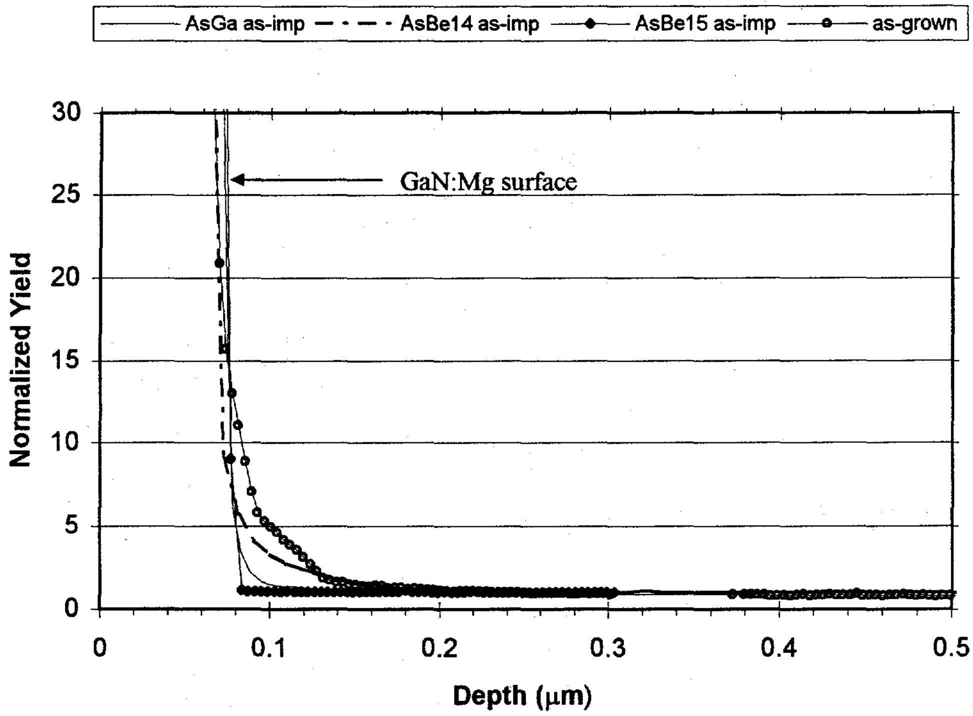

Figure 3.26. Oxygen SIMS depth profiles for the near surface region of the as-grown and as-implanted GaN layers.

The oxygen SIMS profiles for annealed samples are shown in figures 3.27 and 3.28. In both figures the oxygen profiles near the surface of the samples annealed at 1500°C for 30s distinctively show a diffusion related profile. Although it appears as if there was a higher concentration of oxygen in the near surface region of the sample annealed at 1400°C for 60s than near the surface of the as-implanted sample, the shape of the profile does not follow a typical diffusion-tail. Rather, it may be that during sputtering of the surface for SIMS depth profiling, oxygen was knocked in, which caused the surface profile to broaden. The surface profile of the sample annealed at 1400°C for 60s showed similar broadening as the as-grown profile.

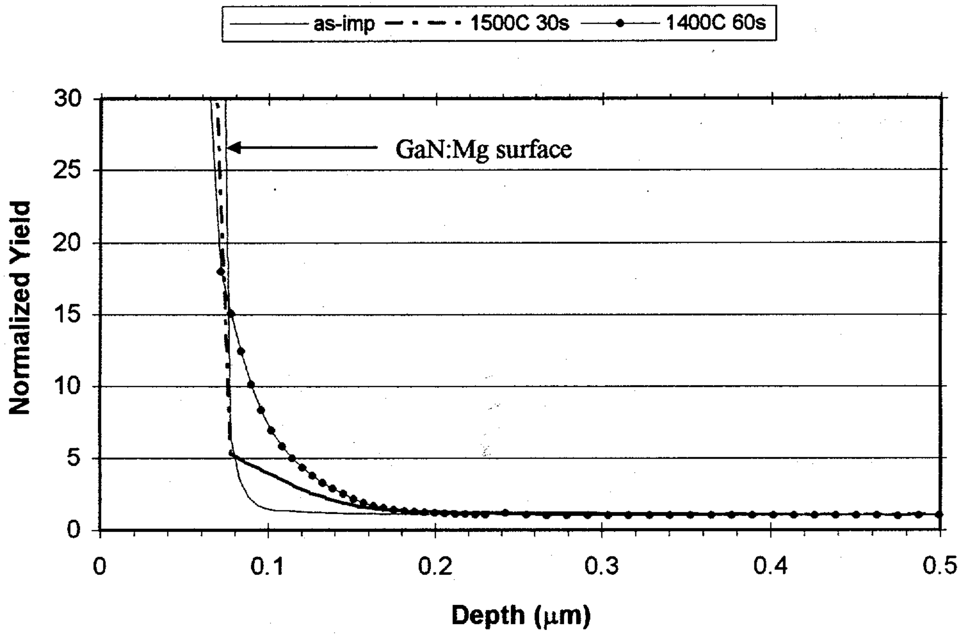

Figure 3.27. Oxygen depth profile for the near surface region of as-implanted and annealed p-GaN implanted with As and Ga.

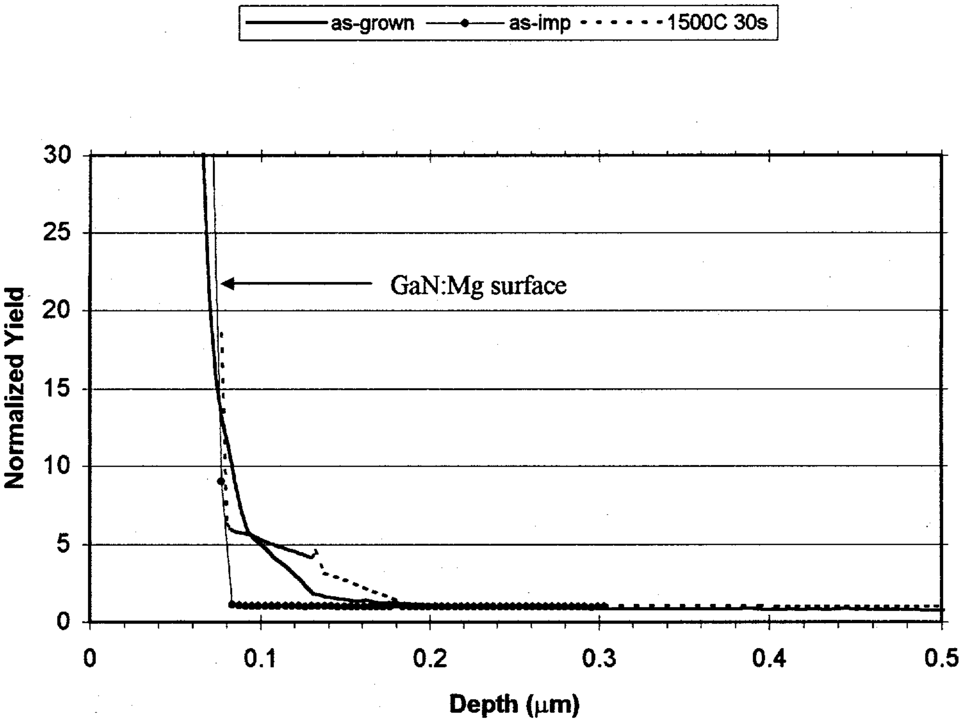

Figure 3.28. Oxygen depth profile for the near surface region of as-implanted and annealed p-GaN implanted with As and Be.

Breakdown of the sapphire substrate may occur during high temperature annealing, and diffusion of oxygen from the substrate into the GaN film was also investigated by SIMS. Figure 3.29 shows the oxygen profiles near the GaN/sapphire interface for an unannealed sample, a sample annealed at 1400°C for 60s and two different samples annealed at 1500°C for 30s labeled (1) and (2). The oxygen profile of the sample annealed at 1400°C for 60s did not show a measurable change as compared to the material which was not annealed. However, like oxygen diffusion from the AlN cap into the surface, oxygen diffusion from the substrate into the GaN layer occured at 1500°C.

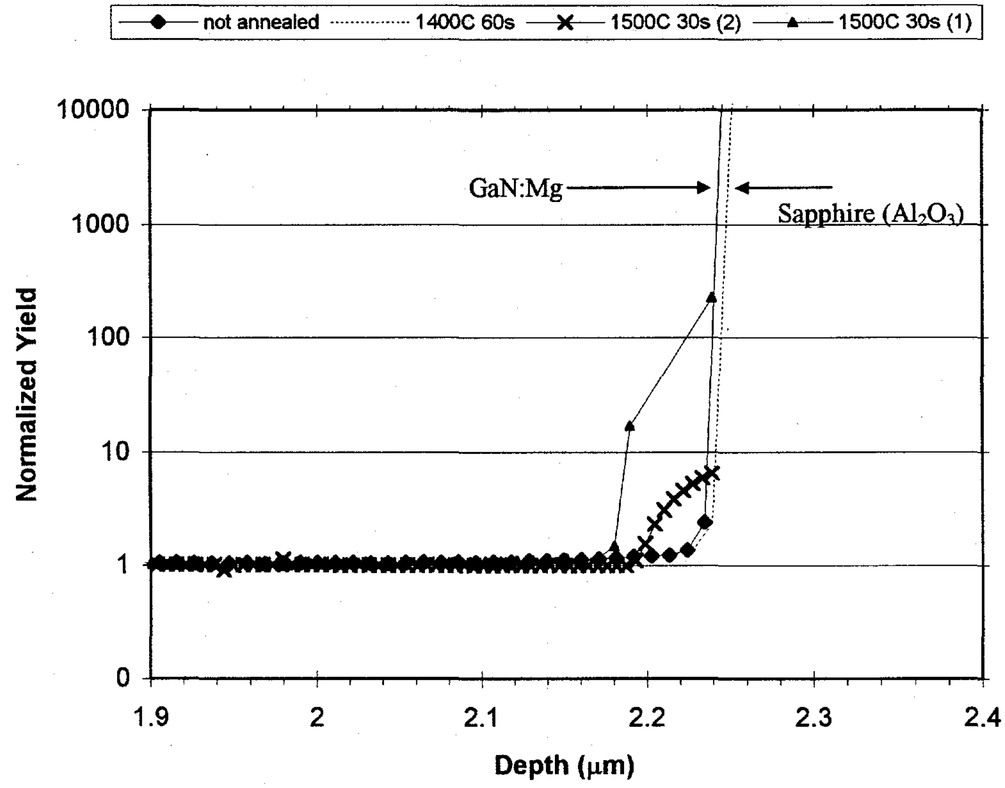

Figure 3.29. SIMS profile of oxygen at the GaN/sapphire interface before and after annealing at 1400°C for 60s and at 1500°C for 30s.

3.5 Diffusion of impurities

Several studies reported in the literature were conducted to understand the redistribution of implanted impurities via diffusion during high temperature annealing. Amongst the studies reported in the literature, there were conflicting observations about the redistribution of some impurities. In all these studies, impurities were first implanted and then annealed. The impurity depth profiles were measured by SIMS. Ca, O, C and Si were consistently reported to have had no measurable redistribution of their depth profiles after annealing i.e., diffusion had not taken place (Wilson et al., 1995; Zolper et al., 1996; Zolper et al., 1997; Cao et al., 1999). Ca and O redistribution was studied after annealing at 1125°C, while C profiles were measured after annealing at temperatures up to 1400°C, and Si was studied after annealing at temperatures up to 1050°C.

Observations about Be, Zn, Mg, S and Se redistribution via diffusion after annealing differed between experimenters. Of these impurities, only Be and Mg are of interest to our studies. Cao et al. (1999) reported broadening of the Be concentration profile after annealing at 900°C with no further motion with annealing up to 1200°C. Zolper (1997) on the other hand, observed no movement of the Be concentration profile after annealing at 1125°C. Conflicting reports about Mg diffusion during annealing were made as well. In Zolper's studies (1997), Mg showed movement towards the surface after annealing at 1125°C. Cao et al. (1999) reported no redistribution of the implanted Mg impurities after annealing at 1450°C. The samples used in the work by Cao et al. were capped with an AlN layer prior to annealing, whereas an AlN capping layer was not mentioned in Zolper's work. It is possible that the AlN cap prevented outdiffusion of Mg during annealing.

In our studies, As, Be and Mg depth profiles were measured after implantation and after annealing to determine if there was a change in the concentration profiles caused by annealing. No movement of the Be concentration profiles within the accuracy of SIMS analysis was detected after annealing at 900°C for 10 minutes and 1400°C for 30s as shown in figure 3.30; the profiles overlap. No redistribution was observed in As implanted samples as well after annealing at 1400°C for 60s and at 1500°C for 30s; the as-implanted and annealed SIMS depth profiles overlap as shown in figure 3.31. Determination of Mg diffusion in the sample was inconclusive because Mg was grown into the samples at a constant concentration. There were no features in the Mg depth profiles to compare.

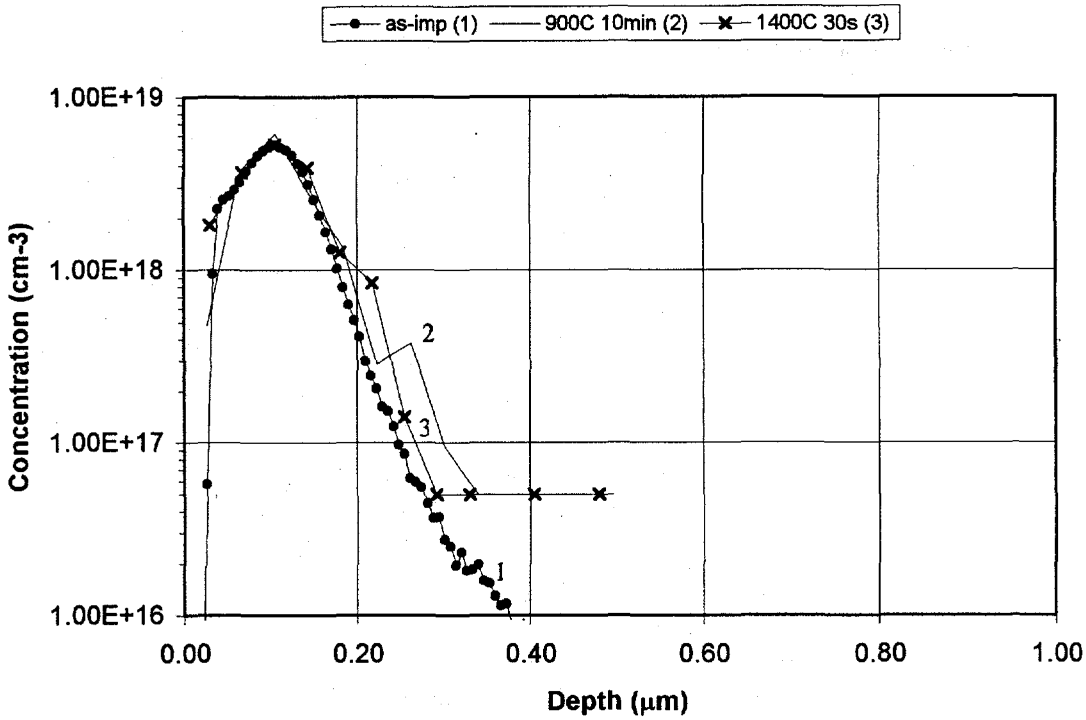

Figure 3.30. SIMS profiles of Be-implanted and annealed GaN.

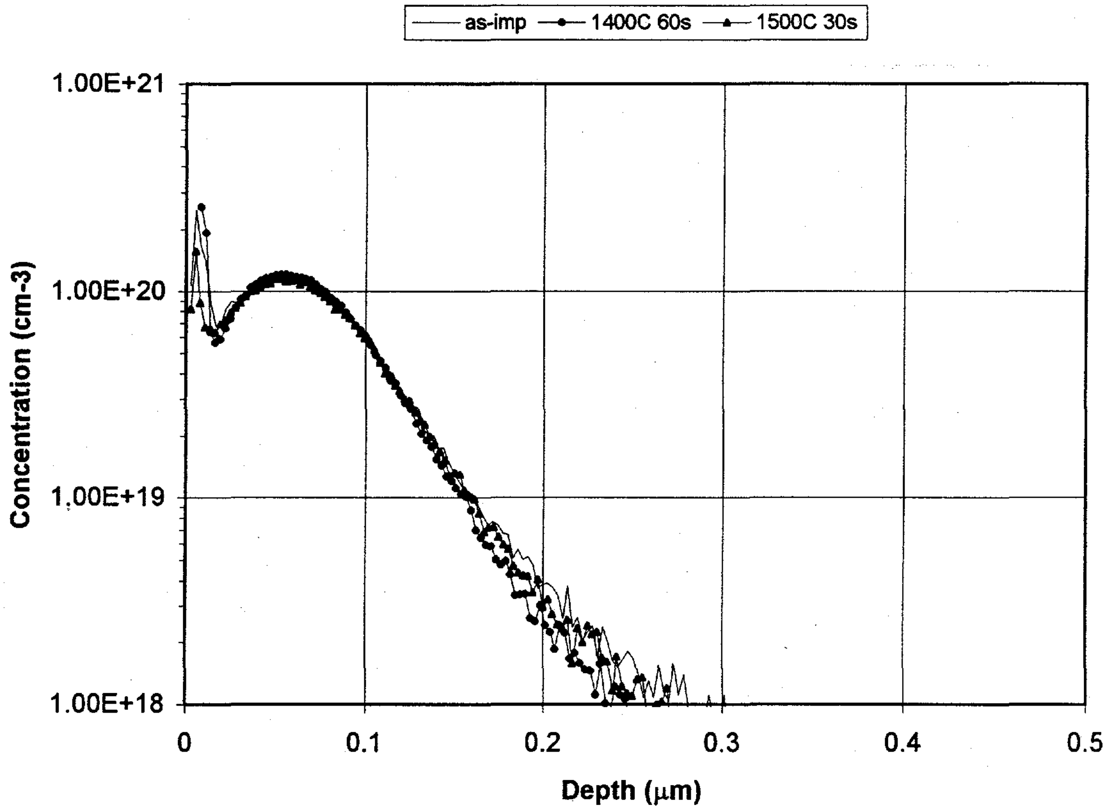

Figure 3.31. SIMS As-depth profiles of As-implanted and annealed GaN.

4. Discussion and conclusions

After implantation of As, As + Be, and As + Ga into GaN and annealing for short durations at temperatures as high as 1500°C, the GaN films remained highly resistive. It was apparent from c-RBS studies that although implantation damage did not create an amorphous layer in the GaN film, annealing at 1500°C did not provide enough energy to completely recover the radiation damage. Disorder recovered significantly after annealing at temperatures up to 1500°C, but not completely. From SIMS analysis, oxygen contamination in the AlN capping layer causes oxygen diffusion into the GaN film above 1400°C. The sapphire substrate (Al_20_3) also decomposed and oxygen penetrated into the backside of the GaN layer above 1400°C. To prevent donor-like oxygen impurities from the capping layer and the substrate from contaminating the GaN film and compensating acceptors, post-implantation annealing should be done at temperatures below 1500°C. Oxygen in the cap could be reduced by growing the AlN cap on the GaN layer after the GaN growth run or by depositing the AlN layer in a ultra high vacuum (UHV) system post-growth to minimize residual oxygen and water contamination. With longer annealing times at 1400°C or at higher temperatures with a higher quality AlN, the implantation damage may fully recover.

Because the films remained highly resistive even after high temperature annealing, the impact of Be incorporation on the electrical transport properties could not be assessed. Even the PL data did not reveal any new Be-related peaks to either support existing findings in the literature or to identify a new and different transition.. From the current studies reported here, co-implantation of Be with As did not enhance the formation of Be acceptors optically, although it still remains unknown if Be forms acceptors in GaN.

A new peak emission in the PL spectra of As-implanted samples occurred at ~2.3 eV. Observing the trends of damage removal and a relative increase in the ~2.3 eV PL peak with increased annealing temperature, it is possible that this peak is not damage related. However it is also possible that this emission is the infamous yellow luminescence which may be due to Ga-vacancies and Ga-vacancy complexes. These two effects may be better differentiated by studying noble gas implants in GaN.

The preliminary hydrogenation experiments of the Be-implanted samples did not yield an improvement in Be-activation. Diffusion of hydrogen into the GaN film was limited to the first 300Å of the layer. This was probably due to the remaining damage in the layer extending from ~200Å to ~1000Å, visible in the c-RBS spectra. The remaining damage peak evident in the c-RBS spectra is large in height and originates from the large amount of planar damage in the film. The hydrogen may pile up and decorate at these accumulated defects which prevents hydrogen from diffusing deeper. Again, complete damage removal is essential to attaining hydrogen diffusion to Be-implanted depths to in turn achieve the neutralization of possible Be acceptors. A better assessment of hydrogen passivation of Be could be made if more of the damage in the films is recovered.

When post-implantation thermal annealing temperatures are increased such that complete implantation damage recovery occurs, optical and electrical properties of Be impurities can be better evaluated. It is apparent from the studies reported here that the remaining damage in the films limits the effects of both the hydrogenation and the activation of Be as acceptors.

5. Future work

Although the work reported here has not yet determined Be to be a shallower p-type dopant in GaN than Mg, it is important to realize that the results of our preliminary studies are the foundations for future work. Most obviously the limiting factor to our study of Be in GaN is implantation damage. The c-RBS measurements have shown that damage removal in the implanted samples by annealing is limited by the decomposition of the GaN surface and the effectiveness of the AlN cap used. Although nearly complete recovery of radiation damage occurs during annealing under the extreme conditions applied here, diffusion of oxygen from the capping layer occurs during annealing at 1500°C. It is apparent that the current method of depositing the AlN cap can incorporate potentially detrimental oxygen thereby limiting the post-implantation annealing temperature. As discussed in the previous section a better method of depositing an AlN cap such as in an MBE system or in the MOCVD reactor after GaN growth may be necessary.

In the studies reported here, p-type GaN with a significant concentration of Mg was used. If Be is an acceptor in GaN, the activation efficiency of the implanted Be may not be optimized under current annealing conditions and the Be acceptor effects may be masked by the high as-grown p-type concentration. In future studies either undoped or lightly doped GaN should be used such that the possible Be acceptors dominate the transport properties. Optimally, Be in GaN is best studied if Be is grown in during MOCVD or MBE growth. This would eliminate the hurdle of overcoming radiation damage and its affects on other processing steps. In the future it may be possible to grow GaN:Be in our MOCVD system to study this. However, currently implantation effects cannot be avoided. Because implantation damage effects the success of acceptor neutralization by hydrogen diffusion from a plasma, co-implantation of hydrogen at depths and concentrations coinciding with Be implants should be considered. The light mass of hydrogen would not create any significant amount of damage compared to the existing implantation damage.

A new peak centered around 2.3 eV in the PL spectra after implantation is reported in this work. It is inconclusive from our current studies whether this peak is related to damage and is the commonly referred to "yellow luminescence" or if this peak is related to As implantation. Implantation of noble gases may resolve this question. It is also possible to co-implant Be with P, another group V element, to determine the origins of the 2.3 eV PL peak. The advantage of implanting P as compared to As is that it is a lighter element which would not create as much damage, however, because P is less massive than As not as many Ga sites for Be substitution may be created.

6. Appendices

6.1 Work functions of selected metals

(Handbook of Chemistry and Physics, 71st ed., 1990)

Element	Work function ϕ_m (experimental value in eV)
Ag	4.26
Al	4.28
Au	5.10
Co	5.00
Cr	4.50
Cu	4.65
Fe	4.50
Ga	4.20
Hg	4.49
In	4.12
Mo	4.60
Ni	5.15
Pd	5.12
Pt	5.65
Ta	4.25
Ti	4.33
W	4.55
Zr	4.05

6.2 Implantation parameters

Sample series	Implant species	Energy (keV)	Dose (atoms cm^{-3})
AsBe14 series	As Be	200 21	1×10^{15} 1×10^{14}
AsBe15 series	As Be	200 21	1×10^{15} 1×10^{15}
As series	As	200	1×10^{15}
AsGa series	As Ga	200 200	1×10^{15} 1×10^{15}

6.3 Characterization techniques

6.3.1 Hall effect and resistivity measurements

The Hall effect is commonly used to characterize the free carrier concentrations in semiconductors and metals. The Hall effect arises from the displacement of charged carriers moving with velocity v in a magnetic field $\mathbf{B}$. The moving charged carriers with charge q will feel a Lorentz force $\mathbf{F}$.

$$\mathbf{F} = q(v x \mathbf{B}) \tag{6.1}$$

This Lorentz force deflects the moving charged particles which then set up an internal electric field perpendicular to both the magnetic field and current. This induced electric field is the Hall field $\mathbf{E}_H$. Figure 6.1 and 6.2 depict the Hall effect for both n- and p-type materials.

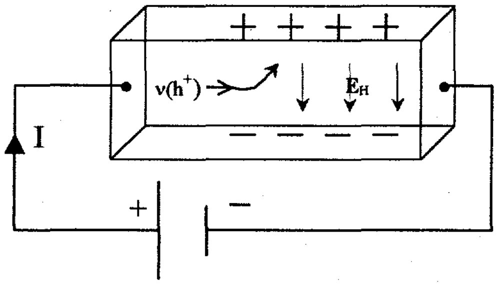

Figure 6.1. Hall effect in p-type material

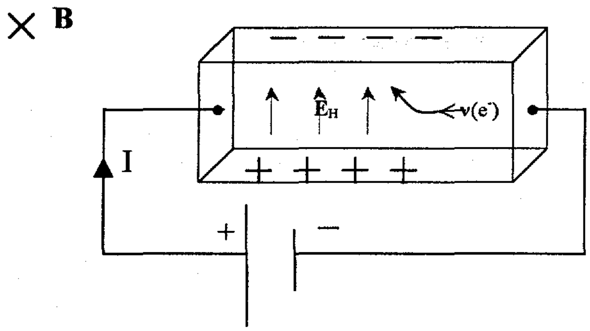

Figure 6.2. Hall effect in n-type material

In equilibrium the induced Hall field will balance the Lorentz force exactly and all charge carriers will move through the sample unaffected by the Lorentz force. Therefore at equilibrium we find:

$$q(v x \mathbf{B}) = q\mathbf{E}_H . \tag{6.2}$$

Current density is defined as **J**=nqv where n is the carrier concentration when conduction is dominated by one type of carrier. Then

$$\mathbf{E}_H = \frac{\mathbf{J}}{nq}\mathbf{B} = R_H\mathbf{JB} \tag{6.3}$$

where

$$R_H = \frac{1}{nq}. \tag{6.4}$$

R_H is the Hall coefficient.

As seen in the figures above, for both n- and p-type material, the majority carriers are displaced in the +z direction by the Lorentz force. A measurement of the voltage across the top and bottom faces yields the Hall voltage, and its sign is determined by the carrier type. For n-type material the Hall field is directed in the +z direction and for p-type material the Hall field is reversed.

The configuration for Hall effect shown in figures 6.1 and 6.2 in which Hall effect measurements are made on a simple Hall bar is not always a convenient geometry. The contacts on the GaN thin film samples studied here were placed on the four corners of each 5x5 mm^2 sample. van der Pauw (van der Pauw, 1958) showed that the Hall effect measurement of an arbitrarily shaped thin film sample could be performed in a simple manner if the sample is continuous, meaning it has no holes, and it has a constant thickness. In addition the contacts have to be small and located at the boundary of the sample, as shown in figure 6.3 below.

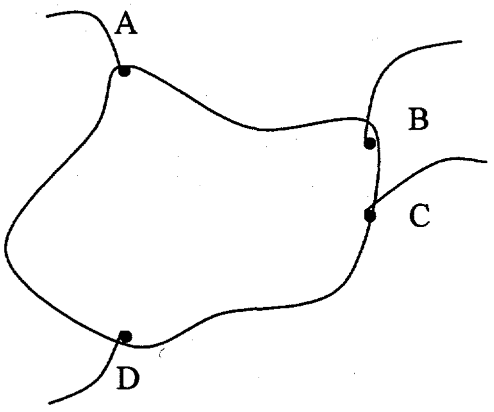

Figure 6.3. Sample of arbitrary shape with contacts at the perimeter.

van der Pauw showed by conformal mapping of the lamellae into a semi-infinite plane that measuring the resistances $R_{AB,CD}$ and $R_{BC,DA}$ and knowing the thickness, resistivity can be expressed by the following equation.

$$\rho = \frac{\pi d}{\ln 2} \frac{\left(R_{AB,CD} + R_{BC,DA}\right)}{2} f\left(\frac{R_{AB,CD}}{R_{BC,DA}}\right) \qquad (6.5)$$

where $R_{AB,CD}$ represents the resistance measured by passing current through contacts A and B and measuring the voltage drop across contacts C and D.

$$R_{AB,CD} = \frac{V_{CD}}{I_{AB}}, \qquad (6.6)$$

and similarly for $R_{BC,DA}$:

$$R_{BC,DA} = \frac{V_{DA}}{I_{BC}}. \qquad (6.7)$$

The function f in equation 6.5 is a correction factor, and it is dependent on the symmetry. The factor f depends on the ratio $R_{AB,CD}$ / $R_{BC,DA}$, satisfying the relation

$$\frac{R_{AB,CD} - R_{BC,DA}}{R_{AB,CD} + R_{BC,DA}} = f \operatorname{arccos} h \left\{ \frac{\exp\left(\frac{\ln 2}{f}\right)}{2} \right\} . \qquad \text{(C.8)}$$

This function is shown in the figure 6.4.

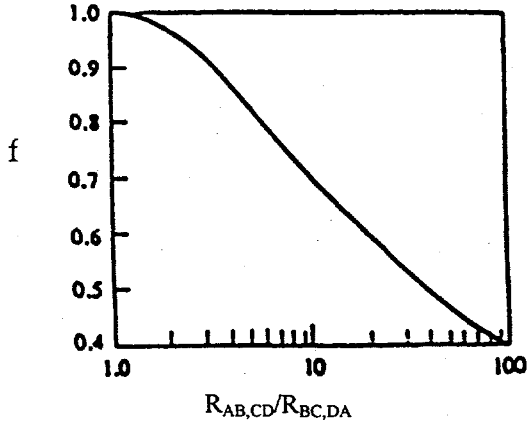

Figure 6.4. Function f plotted as a function of the ratio $R_{AB,CD}/R_{BC,DA}$.

6.3.2 Photoluminescence (PL)

Photoluminescence (PL) is a highly sensitive non-destructive technique which is used to characterize the optically induced radiative recombination transitions of a semiconductor. PL can be used to qualitatively analyze the sample quality and composition, as well as to determine impurities, defects, band gap and carrier lifetimes of a material. Because there are a large number of effects involved in the generation of an electron-hole recombination event, results from photoluminescence are more qualitative in nature than quantitative.

Photoluminescence of direct bandgap semiconductors is a near surface sensitive technique, probing depths of up to ~1000 Å beneath the surface. This sensitivity is dependent on the optical penetration of the stimulating laser light in a particular material and the free carrier diffusion length. Very small sample volumes or low concentrations of defects and impurities can be analyzed due to its high sensitivity.

Photoluminescence requires light with energy greater than the semiconductor band gap, generally 0.6 – 6 eV. The incident photons excite electrons from the valence band into the conduction band. The system can relax non-radiatively by emission of phonons, moving the excited electrons to a lower energy and more stable excited state such as the bottom of the conduction band or an impurity state. The electrons and holes may also form excitons, a weakly bound state of an electron and a hole, which may be free or bound to defects such as acceptors, donors, vacancies, etc. The electron and hole will recombine with a characteristic time constant called lifetime, releasing their energy in the form of a photon. In luminescent materials, radiative emission of the energy is detected, and its intensity is analyzed as a function of the wavelength of emitted light. The emitted light is focused into a spectometer and measured by an optical detector.

Near the bandedge, exciton-related emissions generally dominate the luminescence spectrum. The exciton-related recombinations in GaN that are well understood are the free-excitons A, B and C (FXA, FXB and FXC), the donor-bound exciton (DX) and the acceptor-bound exciton (AX). FXA, FXB and FXC appear at 3.474 eV, 3.481 eV and 3.501 eV respectively (Dingle et al., 1971) and decrease in intensity from A to C. The donor bound exciton peak, DX, is related to an exciton bound to an intrinsic donor and its peak position lies at 3.467 eV in unstrained GaN layers (Kisielowski et al., 1996). DX peaks are typically positioned ~6meV in energy less than the FXA peak, and generally two LO phonon replica lines ~91 meV apart are observed to accompany it. The acceptor bound exciton peak (AX) arises from excitons bound to neutral acceptors. It has a peak position at 3.454 eV (Viswanath et al., 1998), and it is generally very weak in intensity.

Another feature often observed in PL spectra of GaN is a broad band emission centered at ~2.2eV, and it is generally referred to as "yellow luminescence." The source of the yellow luminescence band is not well understood and remains widely debated. However, its presence and intensity are often viewed as an indicator of poor quality films. Several explanations about the origin of the yellow luminescence have been suggested. Some have linked deep C acceptors to the origin of the yellow luminescence (Ogino and Aoki, 1980) while others support deep acceptor Ga vacancies (V_{Ga}) as the defect related source of yellow luminescence (Van de Walle and Neugebauer, 1997). Other interpretations as of the source of yellow luminescence have surfaced, but most reports tend to point to a deep acceptor as the root cause. Van de Walle and Neugebauer (1997) also suggest that V_{Ga}-donor complexes give rise to this luminescence.

6.3.3 Rutherford Backscattering Spectrometry (RBS) and channeling RBS

RBS is a useful technique to quantitatively characterize the matrix and impurity elemental identity, areal concentration and depth distribution, film thickness and crystal quality of a thin film. This technique does not require standards. Additionally, RBS is a relatively non-destructive technique; there is some radiation damage in the area where the beam impinges on the sample, but there is no loss of material as in Secondary Ion Mass Spectrometry where sputtering is required to obtain depth concentration profiles.

RBS utilizes elastic nuclear collisions of high-energy low mass ions with sample atoms. Most high-energy ions projected at the sample lose their energy by electronic collisions, electronic excitation and ionization of target atoms. The few backscattered ions are then analyzed for their energy losses.

Ions for use in RBS, typically He+ or in special cases protons, are accelerated by a high voltage Van de Graaff accelerator to an energy one to two MeV. The high-energy ions are focused and collimated. The beam is directed onto the sample. The energy of the backscattered ions is measured by a solid state detector, and the charged pulses are sorted by energy in a multichannel analyzer. With RBS, elemental identity, concentration and depth profile can be determined generally within an accuracy of a few percent.

There are three fundamental parameters of RBS. The kinematic factor K is the ratio of the energy of the backscattered ion, E_1, and the energy of the incoming ion, E_0. Using the conservation of energy and momentum, this ratio can be determined and yields:

$$K = \frac{E_1}{E_0} = \left[\frac{\left(1 - \left({}^{M_1}\!/\!{}_{M_2}\right)^2 \sin^2\Theta\right)^{\frac{1}{2}} + \left({}^{M_1}\!/\!{}_{M_2}\right)\cos\Theta}{1 + \left({}^{M_1}\!/\!{}_{M_2}\right)} \right]^2 \tag{6.9}$$

M_1 and M_2 are the masses of the incident ion and the target atom respectively, and Θ is the scattering angle between the transmitted beam and the detector as shown in figure 6.5. Mass determination and therefore identity of target atoms can be deduced using equation 6.9.

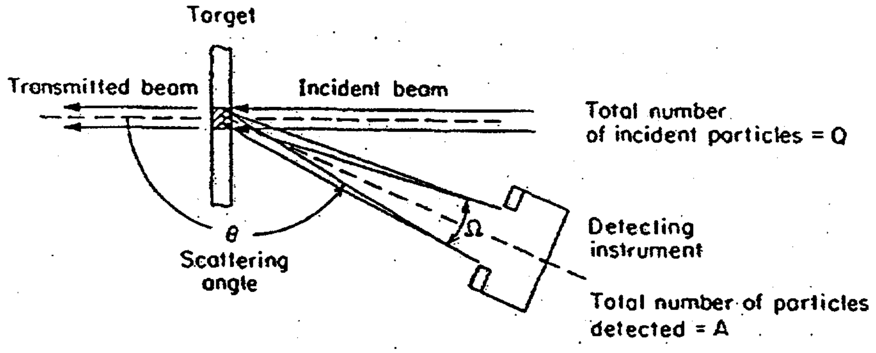

Figure 6.5. Schematic of RBS setup.

The differential scattering cross section, $\frac{d\sigma}{d\Omega}$, is the cross-section for the incident ion to be scattered into dΩ, and it provides quantitative information about the target atoms which are studied.

$$\frac{d\sigma}{d\Omega} = \left(\frac{Z_1 Z_2 e^2}{4E}\right)^2 \frac{4\{[1-((M_1/M_2)\sin\Theta)^2]^{1/2} + \cos\Theta\}}{\sin^4\Theta[1-((M_1/M_2)\sin\Theta)^2]^{1/2}} \tag{6.10}$$

Z_1 and Z_2 are the atomic numbers of the incident and target atoms respectively, dΩ is the differential acceptance angle of the detector and E is the energy of the incident ions before scattering. The probability $\frac{d\sigma}{d\Omega}$ is directly proportional to the square of the incident and target atomic numbers, i.e., a higher atomic number target atom will have a higher probability of backscattering the incoming low mass ion into the detector. As a consequence, sensitivity to higher mass elements is greater than to lower mass elements. The number of backscattered ions from an element, A, is proportional to its concentration, N, where Q is the number of particles incident on the target and t is the target thickness.

$$A = \frac{d\sigma}{d\Omega} * d\Omega * Nt * Q \tag{6.11}$$

The third set of important parameters is differential energy loss $\frac{dE}{dx}$, and the closely related stopping cross section ε. These parameters allow the determination of the depth distribution of target atoms. Energy is lost by two processes, electronic stopping and nuclear stopping. Effective stopping cross section, $[\varepsilon_0]$, and power, $[s_0]$, are given by the equations below.

$$[\varepsilon_0] = \left(\frac{K\varepsilon(E_0)}{\cos\Theta_1} + \frac{\varepsilon(KE_0)}{\cos\Theta_2} \right) \tag{6.12}$$

$$[s_0] = N \cdot [\varepsilon_0] \tag{6.13}$$

$$\Delta E = [s_0] \cdot t \tag{6.14}$$

where ΔE is the difference in energy of ions backscattered from the surface and ions backscattered from depth t.

Figure 6.6 shows a sample RBS spectrum for a thin film of Au on a Si substrate. The area under the Au peak is the number of He ions backscattered from Au atoms, and the energy-width of the Au peak represents the thickness of the gold film. The onset of the Si peak is displaced from $K_{Si}E_0$ by ΔE_{Si}^{Au}, the change in energy of backscattered He ions from the Au signal.

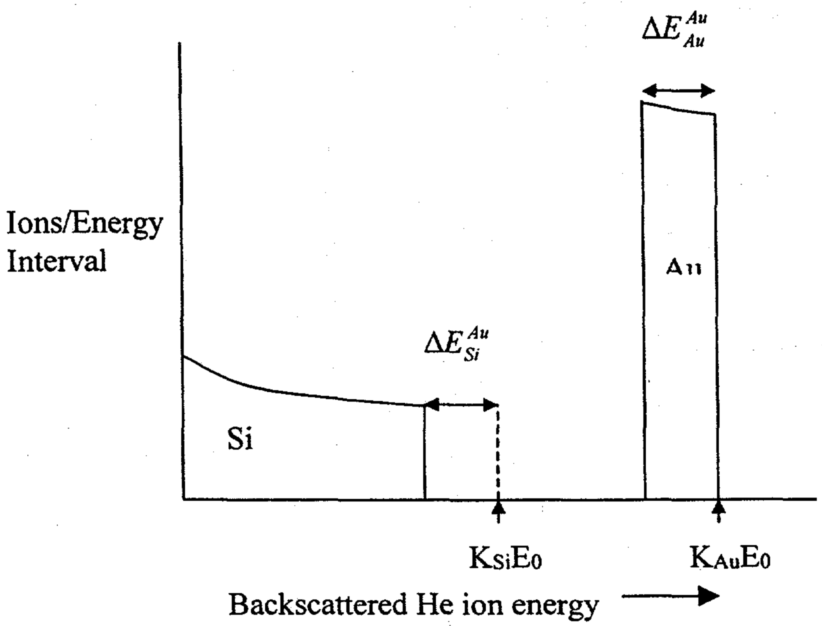

Figure 6.6. Sample RBS spectrum of a Au thin film on Si.

In channeling RBS, the He ion beam is aligned along a low index crystallographic axis. The RBS signal is reduced in the channeling configuration because the probability of direct backscattering from atoms is minimized. Along certain directions in a crystal there are channels along which the incident ions can penetrate deep into the sample because the coulomb repulsion between the incoming ions and the host atoms steer the incoming ions along the channel. These channeled ions lose energy by electronic interactions with the lattice more than by nuclear interactions. Channeled ions will penetrate deeper into a crystalline sample than in an amorphous target.

By using the channeling orientation, crystallographic information of radiation damaged samples can be determined. If there is disorder in a crystal such as point and line defects, the backscattering yield in channeling orientation will be larger than the yield from a crystal without defects. This is because the ions in the incident beam will scatter at defects like atoms displaced into a channel instead of penetrating deeper into the crystal along the channel. If the sample is amorphous, the backscatter yield will equal the random yield.

To determine the crystalline quality of radiation damaged samples, the c-RBS spectra of the implanted films can be compared to the c-RBS spectra of non-implanted films as well as a random spectrum. An increase in backscatter yield from implanted samples indicates quantitatively the number of displaced host atoms. The energy width of the increased backscatter peak indicates the depth of damage, and by integrating over the damage peak and subtracting the channeling backscatter yield of the non-implanted sample, the number of displaced host atoms can be determined.

6.3.4 Secondary Ion Mass Spectrometry (SIMS)

SIMS is a highly sensitive chemical analysis technique that can detect all elements, H through U, and any isotope of any element in a material present at levels in the ppb range, generally at concentrations as low as $10^{12} - 10^{16}$ cm^{-3}. The SIMS technique is dependent on the detection and identification of ejected charged particles when ions of medium energy are incident on a sample. Typically the primary ion beam consists of oxygen, cesium or argon ions with energy between 1 and 20 keV and a current of 10 nA to 15 μA. Generally, the oxygen beam is used to enhance the backscattering yield of electropositive elements, and the cesium beam is used to enhance the yield of electronegative elements.

In SIMS, the primary beam is incident on the sample, and through a series of direct or indirect collisions, the energy and momentum from the incident ions are transferred to near surface atoms. Transfer of the energy and momentum from the primary beam to the sample causes ejection of neutral and charged species, resulting in sputtering of the surface. Only charged ejected particles are useful for SIMS detection because they can be mass analyzed. Therefore, the detection limits for individual elements vary depending on the efficiency of ionization of each element. The higher the ionization efficiency, the lower the detection limit. This ionization efficiency is dependent on the electron affinity of positive ions or the ionization potential of negative ions.

As sputtering of the sample surface continues, a crater is formed and a depth profile can be determined. To preserve the depth resolution of the profile the primary ions are rastered over a small sample area, and secondary ions are collected from the center of the bottom of the crater. This is achieved by the use of electronic gating or a physical aperture in the mass spectrometer which rejects the secondary ions emitted from the crater walls representing material from different depths. The secondary ions collected are then filtered by energy and separated as a function of their mass to charge ratio by a magnet in the mass spectrometer.

A depth profile is typically collected as secondary ion count as a function of time. Time can be translated into depth after the depth of the crater has been physically measured. If the sputter rate during SIMS is kept constant an accurate assignment of depth can be made. The secondary ion count is translated into concentration by the use of standards.

The depth resolution of SIMS is dependent on the depth of the region into which the incident ions mix with displaced atoms. The thickness of this region is dependent on the mass, energy and incidence angle of the primary beam as well as on the sample itself. By increasing the mass of the primary ions or by decreasing the energy or incidence angle, the depth of this region is reduced, thereby increasing the depth resolution. The surface roughness of the sample also affects the depth resolution; a rough sample surface will degrade the depth resolution. Decreasing the sputter rate can also enhance depth resolution. However, this will adversely affect the detection limits of species. By increasing the sputter rate, more ions are ejected and measured per unit time, thereby lowering the detection limit but compromising depth resolution.

7. References

H. Amano, M. Kito, K. Hiramatsu and I. Akasaki, Jpn. J. Appl.Phys. **28**, L2112 (1989).

A. Baldereschi and N.O. Lipar, Physics of Semiconductors Proc. of the 13th Int. Conf. 595 (1976).

P. Bergman, G. Ying, B. Monemar and P.O. Holtz, J. Appl. Phys. **61**, 4589 (1987).

F. Bernardini, V. Fiorentini and A. Bosin, Appl. Phys. Lett. **70**, 2990 (1997).

M.S. Brandt, N.M. Johnson, R.J. Molnar, R. Singh and R.D. Moustakas, Appl. Phys. Lett. **64**, 2264 (1994).

O. Brandt, H. Yang, H. Kostial and K. Ploog, Appl. Phys. Lett. **69**, 2707 (1996).

Encyclopedia of Materials Characterization, edited by C.R. Brundle, C.A. Evans, Jr. and S. Wilson (Buttterworth-Heinemann, Boston, 1992).

X.A. Cao, C.R. Abernathy, R.K. Singh, S.J. Pearton, M. Fu, V. Sarvepalli, J.A. Sekhar, J.C. Zolper, D.J. Rieger, J. Han, T.J. Drummond, R.J. Shul and R.G. Wilson, Appl. Phys. Lett. **73**, 229 (1998).

X.A. Cao, S.J. Pearton, F. Ren and J.R. Lothian, Appl. Phys. Lett. **73**, 942 (1998).

X.A. Cao, R.G. Wilson, J.C. Zolper, S.J. Pearton, J. Han, R.J. Shul, D.J. Reiger, R.K. Singh, M. Fu, V. Scarvepalli, J.A. Sekhar and J.M. Zavada, J. Elec. Mat. **28**, 261 (1999).

D.J. Dewsnip, A.V. Andrianov, I. Harrison, J.W. Orton, D.E. Lacklison, G.B. Ren, S.E. Hooper, T.S. Cheng and C.T. Foxon, Semicond. Sci. Technol. **13**, 500 (1998).

R. Dingle, D.D. Sell, S.E. Stokowski and M. Ilegems, Phys. Rev. B **4**, 1211 (1971).

K.J. Duxstad, PhD Thesis, University of California-Berkeley, 1997.

C.J. Eiting, P.A. Grudowski, R.D. Dupuis, H. Hsia, Z. Tang, D. Becher, H. Kuo, G.E. Stillman and M. Feng, Appl. Phys. Lett. **73**, 3875 (1998).

W. Götz, N.M. Johnson, D.P. Bour, M.D. McCluskey and E.E. Haller, Appl. Phys. Lett. **69**, 3725 (1996).

W. Götz, N.M. Johnson, J. Walker and D.P. Bour, Mat. Res. Soc. Symp. Proc. **423**, 595 (1996).

R. Groh, G. Gerey, L. Bartha and J.I. Pankove, Phys. Stat. Sol. (a) **26**, 353 (1974).

J. Ho, C. Jong, C.C. Chiu, C. Huang, C. Chen and K. Shih, Appl. Phys. Lett. **74**, 1275 (1999).

M. Ilegems and R. Dingle, J. Appl. Phys. **44**, 4234 (1973).

D.B. Ingerly, Y.A. Chang and Y. Chen, Appl. Phys. Lett. **74**, 2480 (1999).

H. Ishikawa, S. Kobayashi, Y. Koide, S. Yamasaki, S. Nagai, J. Umezaki, M. Koike and M. Murakami, J. Appl. Phys. **81**, 1315 (1997).
W.M. Jadwisienczak and H.J. Lozykowski, Mat. Res. Soc. Symp. Proc. **482**, 1033 (1998).

J. Jang, I. Chang, H. Kim, T. Seong, S. Lee and S. Park, Appl. Phys. Lett. **74**, 70 (1999).

N. Johnson, W. Götz, J. Neugebauer and C.G. Van de Walle, Mat. Res. Soc. Symp. Proc. **395**, 723 (1996).

H. Katayama-Yoshida and T. Yamamoto, Phys. Stat. Sol. (b) **202**, 763 (1997).

C. Kisielowski, J. Krüger, S. Ruvimov, T. Suski, J.W. Ager III, E. Jones, Z. Liliental-Weber, M. Rubin and E.R. Weber, Phys. Rev. B **54**, 17745 (1996).

T. Kim, J. Khim, S. Chae and T. Kim, Mat. Res. Soc. Symp. Proc. **468**, 427 (1997).

J.K. Kim, J. Lee, J.W. Lee, H.E. Shin, Y.J. Park and T. Kim, Appl. Phys. Lett. **73**, 2953 (1998).

D.J. King, L. Zhang, J.C. Ramer, S.D. Hersee and L.F. Lester, Mat. Res. Soc. Symp. Proc. **468**, 421 (1997).

J. Lee, M. Wever, J.K. Kim, J.W. Lee, Y.J. Park, T. Kim and K. Lynn, Appl. Phys. Lett. **74**, 2289 (1999).

X. Li, S. Kim, E.E. Reuter, S.G. Bishop and J.J. Coleman, Appl. Phys. Lett. **72**, 1990 (1998).

T. Mattila and A. Zunger, Phys. Rev. B **58**, 1367 (1998).

J.R. Mileham, S.J. Pearton, C.R. Abernathy, J.D. MacKenzie, R.J. Shul and S.P. Kilcoyne, Appl. Phys. Lett. **67**, 1119 (1995).

F. Mireles and S. Ulloa, Phys. Rev. B **58**, 3879 (1998).

A.J. Moll, J.W. Ager, III, K.M. Yu, W. Walukiewicz and E.E. Haller, J. Appl. Phys. **74**, 7118 (1993).

T. Mori, T. Kozawa, T. Ohwaki, Y. Taga, S. Nagai, S. Yamasaki, S. Asami, N. Shibata and M. Koike, Appl. Phys. Lett. **23**, 3537 (1996).

T. Mori, T. Kozawa, T. Ohwaki, Y. Taga, S. Nagai, S. Yamasaki, S. Asami, N. Shibata and M. Koike, Appl. Phys. Lett. **69**, 3537 (1996).

M. Murakami and Y. Koide, Critical Reviews in Solid State and Materials Sciences, **23**, 1 (1998).

S. Nakamura, N. Iwasa, M. Senoh and T. Mukai, Jpn. J. Appl. Phys. **31**, 1258 (1992).
J. Neugebauer and C.G. Van de Walle, Phys. Rev. B **50**, 8067 (1994).

J. Neugebauer and C. Van de Walle, J. Appl. Phys. **85**, 3003 (1999).

Hydrogen in Semiconductors II, edited by N.H. Nickel (Academic Press, San Diego) 1999.

C. Noguez, R. Esquivel-Sirvent, D.R. Alfonso, S.E. Ulloa and D.A. Drabold, Mat. Res. Soc. Symp. Proc. **449**, 991 (1997).

T. Ogino and M. Aoki, Jpn. J. Appl. Phys. **18**, 1049 (1978).

T. Ogino and M. Aoki, Jpn. J. Appl. Phys. **19**, 2395 (1980).

M. Ohring, *The Materials Science of Thin Films* (Academic Press, San Diego), 1992.

Hydrogen in Semiconductors, edited by J. Pankove and N.M. Johnson (Academic Press, San Diego) 1991.

J.I. Pankove and J.A. Hutchby, J. Appl. Phys. **47**, 5387 (1976).

N. Parikh, A. Suvhanov, M. Lioubtchenko, W. Carlson, M. Bremser, D. Bray, R. Davis and J. Hunn, Nuclear Instruments and Methods in Physics Research B **127/128**, 463 (1997).

S.J. Pearton, J.C. Zolper, R.J. Shul and F. Ren, J. Appl. Phys. **86**, 1 (1999).

S. Porowski, J. Jun, P. Perlin, I. Grzegory, H. Teisseyre and T. Suski, Inst. Phys. Conf. Ser. **137**, 369 (1993).

C. Ronning, E.P. Carlson, D.B. Thomson and R.F. Davis, Appl. Phys. Lett. **73**, 1622 (1998).

A. Salvador, W. Kim, O. Aktas, A. Botchkarew, Z. Fan and H. Morkoc, Appl. Phys. Lett. **69**, 2692 (1996).

F.J. Sanchez, F. Calle, M.A. Sanchez-Garcia, E. Calleja, E. Munoz, C.H. Molloy, D.J. Somerford, J.J. Serano and J.M. Bianco, Semicond. Sci. Technol. **13**, 500 (1998).

T. Suski, J. Jun, M. Leszczynski, H. Teisseyre, S. Strite, A. Rockett, A. Pelzmann, M. Kamp and K.J. Ebeling, J. Appl. Phys. **84**, 1155 (1998).

T. Suski, J. Jun, M. Leszczynski, H. Teisseyre, S. Strite, A. Rockett, A. Pelzmann, M. Kamp and K.J. Ebeling, J. Appl. Phys. **84**, 1155 (1998).

A. Salvador, W. Kim, O. Aktas, A. Botchkarew, Z. Fan and H. Morkoc, Appl. Phys. Lett. **69**, 2692 (1996).

J.K. Sheu, Y.K. Su, G.C. Chi, P.L. Koh, M.J. Jou, C.M. Chang, C.C. Liu and W.C. Hung, Appl. Phys. Lett. **74**, 2340 (1999).

L.L. Smith, R.F. Davis, M.J. Kim, R.W. Carpenter and Y. Huang, J. Mater. Res. **12**, 2249 (1997).

A. Suvkhanov, J. Hunn, W. Wu, D. Thomson, K. Price, N. Parikh, E. Irene, R.F. Davis and L. Krasnobaev, Mat. Res. Soc. Symp. Proc. **512**, 475 (1998).

M. Suzuki, T. Kawakami, T. Arai, S. Kobayashi, Y. Koide, T. Uemura, N. Shibata and M. Murakami, Appl. Phys. Lett. **74**, 275 (1999).

H.H. Tan, J.S. Williams, C. Yuan and S.J. Pearton, Mat. Res. Soc. Symp. Proc. **395**, 807 (1996).

H.H. Tan, J.S. Williams, J. Zou, D.J.H. Cockayne, S.J. Pearton, J.C Zolper and R.A. Stall, Appl. Phys. Lett. **72**, 1190 (1998).

C. Van de Walle and J. Neugebauer, Mat. Res. Soc. Symp. Proc. **449**, 861 (1997).

L.J. van der Pauw, Philips Research Reports **13**, 1 (1958).

J.A. Van Vechten, Phys. Rev. B **7**, 1479 (1973).

J.A. Van Vechten, J.D. Zook, R.D. Horning and B. Goldenberg, J. Appl. Phys. **31**, 3662 (1992).

C.B. Vartuli, S.J. Pearton, C.R. Abernathy, J.D. MacKenzie and F. Ren, Solid-State Electronics **4**, 1947 (1997).

A.K. Viswanath, J.I. Lee, S. Yu, D. Kim, Y. Choi and C. Hong, J. Appl. Phys. **84**, 3848 (1998).

W. Walukiewicz, chapter in *Defects in Optoelectronic Materials*, edited by K. Wada and S. Pang (G&B Science Publisher, Newark), 1998.

C. Wetzel, T. Suski, J.W. Ager III, E.R. Weber, E.E. Haller, S. Fischer, B.K. Meyer, R.J. Molnar and P. Perlin, Phys. Rev. Lett. **78**, 3923 (1997)

R.G. Wilson, S.J. Pearton, C.R. Abernathy and J.M. Zavada, Appl. Phys. Lett. **66**, 2238 (1995).

R.W. Wood, Phil. Mag. **44**, 541 (1922).

T. Yamamoto and H. Katayama-Yoshida, Mat. Res. Soc. Symp. Proc. **468**, 105 (1997).

D. Youn, M. Hao, H. Sato, T. Sugahara, Y. Naoi and S. Sakai, Jpn. J. Appl. Phys. **37**, 1768 (1998).

J.C. Zolper, RG. Wilson, S.J. Pearton and R.A. Stall, Appl. Phys. Lett. **68**, 1945 (1996).

J.C. Zolper, D.J. Rieger, A.G. Baca, S.J. Pearton, J.W. Lee and R.A. Stall, Appl. Phys. Lett. **69**, 538 (1996).

J.C. Zolper, J. Crys. Growth **178**, 157 (1997).

J.C. Zolper in *Application of Accelerators in Research and Industry,* edited by J.L Duggan and I.L. Morgan (AIP Press, New York), 1997, pp. 1017-1020.

J.C. Zolper, M.H. Crawford, J.S. Williams, H.H. Tan and R.A. Stall, Nuclear Instruments and Methods in Physics Research B **127**, 467 (1997).

J.C. Zolper, S.J. Pearton, J.S. Williams, H.H. Tan, R.J. Karlicek, Jr. R.A. Stall, Mat. Res. Soc. Symp. Proc. **449**, 981 (1997).

J.C. Zolper, J. Han, R.M. Biefeld, S.B. Van Deusen, W.R. Wampler, D.J. Riger, S.J. Pearton, J.S. Williams, H.H. Tan, R.F. Karlicek, Jr. and R.A. Stall, J. Elec. Mat. **27**, 179 (1998).

J.C. Zolper, J. Han, S.B. Van Deusen, M.H. Crawford, R.M. Biefeld, J. Jun, T. Suski, J.M. Baranowski and S. J. Pearton, Mat. Res. Soc. Symp. Proc. **482**, 979 (1998).